pressed with wild-type HA-Tip60, there was a higher level of Lys5-aceylated H2AX-Flag without γIR-treatment, and the levels also increased following γIR. When co-expressed with HA-Tip60-ad, a mutant that lacks acetylase activity [6], Lys5-acetylated H2AX-Flag was not detected before or after γIR, confirming that acetylation of H2AX on Lys5 following γIR is mediated by Tip60 (Fig. 1C). Next, to examine the effects of the Sirt1 interaction on the Tip60-mediated acetylation of H2AX, we first designed short hairpin RNAs (shRNAs) directed against Tip60 (pSuper-shTip60) or Sirt1 (pSuper-shSirt1) (Fig. S4). The shTip60 reduced the level of acetylated H2AX-Flag and endogenous H2AX on Lys5 both before and after γIR as compared with a scrambled shRNA control (Fig. 1D). On the other hand, shSirt1 led to an increase in the level of acetylated H2AX-Flag and endogenous H2AX on Lys5 before and after γIR (Fig. 1D). More, Overexpression of Sirt1-myc suppressed the γIR-induced acetylation of H2AX-Flag on Lys5 (Fig. S3B). These results indicated that Sirt1 represses Tip60-mediated acetylation of H2AX on Lys5.

Acetylation of H2AX on Lys5 is required for DDR pathway

Next, K5R H2AX-Flag, which should act as a dominant-negative repressor of the acetylation of endogenous H2AX on Lys 5, was expressed in HeLa cells, which were then treated with 5 Gy γ-ray. We measured the proportion of cells with more than 10 MDC1, BRCA1, or Rad51 foci in cells expressing H2AX-Flag or K5R H2AX-Flag following γIR. More than 80% of the mocked- or H2AX-Flag-transfected cells had more than 10 MDC1 or BRCA1 foci, and more than 50% of them had more than 10 Rad51 foci (Fig. 2). In contrast, following γIR, the number of cells overexpressing K5R H2AX-Flag with more than 10 MDC1, BRCA1, or Rad51 foci was greatly reduced after γIR (Fig. 2). As it is likely that K5R H2AX-Flag prevents the acetylation of endogenous H2AX, these results strongly suggest that the acetylation of H2AX on Lys5 is required for IRIF formation and for efficient recruitment of the DSB repair factor Rad51 to DSB sites. Thus Sirt1 appears to repress the acetylation of H2AX on Lys5 to inhibit formation of IRIF and Rad51 foci.

Sirt1 deacetylates auto-acetylated Tip60

To investigate the mechanism of how Sirt1 represses acetylation of H2AX, we examined the effects of γIR on the physical interaction between Tip60 and Sirt1 (Fig. S5A). Unexpectedly, the amount of Sirt1-myc co-immunoprecipitated with Flag-Tip60 was unaffected by γIR. However, γIR strongly affected the level of acetylated Tip60, which is auto-acetylated or is acetylated by p300/CBP [20,21]; that is, the level of acetylated Flag-Tip60 was decreased gradually after approximately 2 h post-γIR and returned to the basal level within 4 h (Fig. S5A).

Additionally, we co-transfected Flag-Tip60 with either Sirt1-myc or H363Y Sirt1-myc and treated each cell culture with 5 Gy γ-ray (Fig. 3A). In the control experiment, acetylated Flag-Tip60 decreased within 2 h after γIR. Co-expression of Sirt1-myc accelerated the decrease of acetylated Flag-Tip60, whereas co-expression of H363Y Sirt1-myc delayed it. Furthermore, depletion of Sirt1 by shSirt1 increased acetylated Flag-Tip60 and recombinant GST-Sirt1-myc effectively deacetylated acetylated Flag-Tip60, confirming that Sirt1 is required for the deacetylation of Tip60 (Fig. S5B and C).

Nicotinamide, which inhibits Sirt1 [13], increased the level of acetylated Tip60 (Fig. 3B), strongly suggesting that Sirt1 deacetylates Tip60. Interestingly, trichostatin A, an inhibitor of class I and II histone deacetylases (HDACs) but not of Sirt1, also increased the level of acetylated Tip60, indicating a collaboration between Sirt1 and class I and II HDACs in the deacetylation of Tip60 (Fig. 3B).

These results indicate that a part of Tip60 is normally acetylated at least, and that Sirt1 deacetylates acetylated Tip60 in response to DNA damage. However, Sirt1 could not deacetylate acetylated H2AX-Flag in the deacetylation assay *in vitro*, suggesting that Sirt1 indirectly regulates the acetylation level of H2AX (Fig. S5D).

Sirt1 regulates the amount of Tip60 protein

The deacetylated form of Foxo3a, which is deacetylated by Sirt1, is less stable than the acetylated one [22]. Thus, we examined

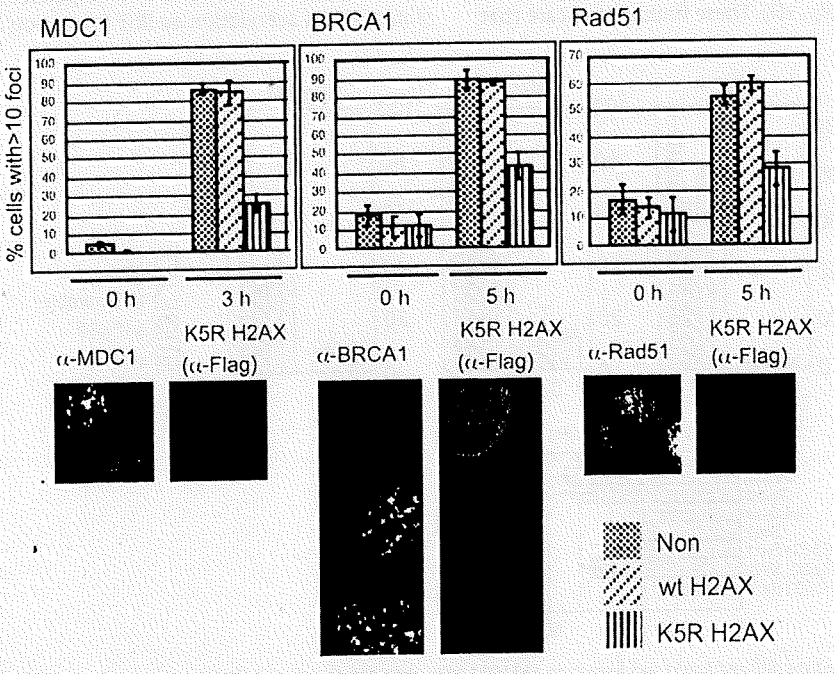

Fig. 2. Acetylation of H2AX on Lys5 is required for IRIF and Rad51 foci formation. HeLa cells were transfected with empty vector (Non) or vectors for wild-type H2AX-Flag (wt) or K5R H2AX-Flag (K5R). After 24 h, cells were seeded on a glass chamber slide. After an additional 24 h, cells were irradiated with 5 Gy of γIR and fixed at the indicated time points. Left panel, anti-MDC1 (α-MDC1); middle panel, anti-BRCA1 (α-BRCA1); right panel, anti-Rad51 (α-Rad51). In all cases, the proportion of cells with more than 10 foci was determined by dividing the number of cells expressing wild-type or K5R H2AX-Flag with more than 10 foci by the total number of cells expressing the exogenous protein. Representatives of three independent experiments are shown, and values represent means ± SE.

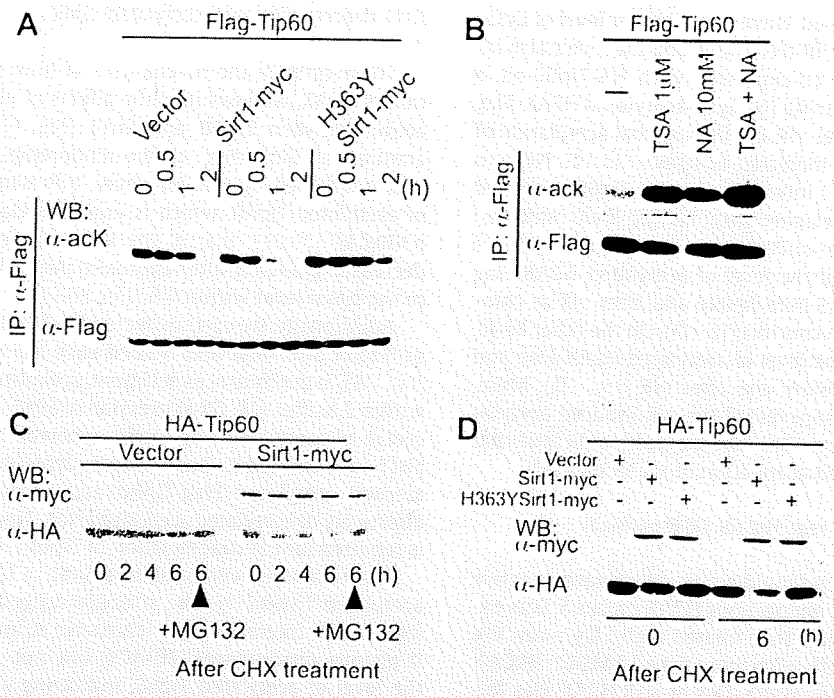

Fig. 3. Sirt1 deacetylates auto-acetylated Tip60 and facilitates proteasome-dependent Tip60 degradation. (A) Sirt1-myc or H363Y Sirt1-myc were transiently co-expressed with Flag-Tip60 in HEK293 cells, and after 48 h, cells were irradiated with 5 Gy of γIR. Cells were then lysed in RIPA buffer for IP of Flag-Tip60 with anti-Flag. (B) HEK293 cells were transfected with Flag-Tip60. After 48 h, cells were treated for 6 h with 1 μM trichostatin A (TSA), 10 mM nicotinamide (NA), or 1 μM TSA and 10 mM NA (TSA + NA). After drug treatment, cells were lysed in RIPA buffer for IP. (C) HA-Tip60 was co-expressed in HEK293 cells with empty vector (mock) or Sirt1-myc. Transfected cells were treated with 10 μM cycloheximide (CHX) for the indicated time. Anti-HA (α-HA) or anti-myc (α-myc) was used as primary antibodies for WB. (D) HA-Tip60 was co-expressed in HEK293 cell with mock (empty) vector, Sirt1-myc vector, or H363Y Sirt1-myc vector. The cells were treated with 10 μM cycloheximide for 6 h.

whether Sirt1 affects the stability of Tip60 in HA-Tip60/Sirt1-myc co-transfected cells (Fig. 3C). When co-expressed with Sirt1-myc, the level of HA-Tip60 decreased more rapidly than when co-expressed with empty vector, suggesting that Tip60 protein is less stable in the presence of excess Sirt1. The decrease in HA-Tip60 protein was suppressed by the proteasome inhibitor MG132 (Fig. 3C). The decrease in HA-Tip60 protein was not enhanced by co-expression of H363Y Sirt1 (Fig. 3D). These findings indicate that Tp60 is degraded in proteasome-dependent manner, and that the deacetylase activity of Sirt1 is necessary for the degradation of Tip60.

Depletion of Sirt1 leads to an increase in IRIF and Rad51 foci formation

We analyzed the effects of endogenous Sirt1-mediated repression of H2AX acetylation on IRIF formation and Rad51, an essential

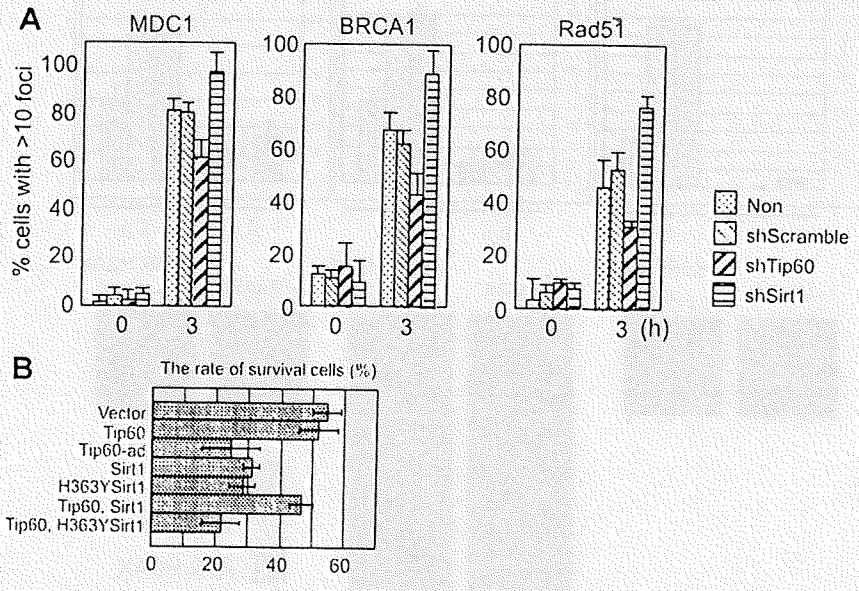

Fig. 4. Tip60 and Sirt1 cooperatively regulate IRIF and Rad51 foci formation. (A) HeLa cells were non-transfected (Non) or transiently transfected with pSuper-shScramble-EGFP (control), pSuper-shTip60-EGFP, or pSuper-shSirt1-EGFP. After 48 h, cells were irradiated with 5 Gy of γIR and then incubated for 3 h. Anti-MDC1, anti-BRCA1, and anti-Rad51 antibodies were used for immunofluorescence microscopy. The proportion of cells with more than 10 foci was calculated by dividing the number of EGFP-positive cells with more than 10 foci by the total number of EGFP-positive cells. Representatives of seven independent experiments are shown, and values represent means ± SE. (B) Cell survival after γIR. HeLa cells expressing different types of protein were treated with 2.5 Gy of γIR. After 2 weeks, cell colonies were counted, and the fraction of surviving cells was calculated.

factor for homologous recombination (HR) [23], recruitment to DSB *in vivo*. For these experiments, Tip60 was depleted with pSuper-shTip60-enhanced green fluorescent protein (EGFP) and Sirt1 was depleted with pSuper-shSirt1-EGFP (Fig. 4A). These constructs allowed cells containing the shRNA construct to be identified by EGFP fluorescence. The proportion of EGFP-positive cells with more than 10 MDC1, BRCA1, or Rad51 foci were the same in cells transfected with the control vector (shScramble-EGFP) as in untransfected cells before or after γIR. However, the proportion of cells with more than 10 MDC1, BRCA1, or Rad51 foci was reduced in Tip60-depleted cells. In contrast, shRNA-mediated depletion of Sirt1 led to a gradual increase in the proportion of cells with more than 10 MDC1, BRCA1, or Rad51 foci, suggesting that Sirt1 normally represses MDC1, BRCA1, or Rad51 foci formation and, together with the results of Fig. 2, that the repression of H2AX acetylation by Sirt1 resulted in a decrease of IRIF and Rad51 foci (Fig. 4A).

Overexpression of Sirt1 results in loss of cellular viability following γIR, which can be rescued by Tip60

Finally, to analyze the association of Sirt1 and Tip60 on cellular survival after γIR, HeLa cells were stably transfected with HA-Tip60 or HA-Tip60-ad and either Sirt1-myc or H363Y Sirt1-myc as shown in Fig. 4B. Expression of HA-Tip60-ad sensitized cells to γIR, indicating that Tip60 activity was required for cellular survival after γIR. Moreover, overexpression of Sirt1-myc reduced the resistance of cells to γIR, indicating that an excess of Sirt1 had deleterious effects on DNA-damaged cells. The effect could be partially rescued by overexpression of HA-Tip60. These results are consistent with the hypothesis that Sitr1 negatively regulates DDR by repressing the activity of Tip60.

Discussion

We showed that Sirt1 physically interacts with Tip60 and that Sirt1 deacetylates auto-acetylated Tip60 and stimulates the proteasome-dependent degradation of Tip60. Although Tip60 plays an important role in DDR through acetylating H2AX on Lys5, Sirt1 represses acetylation of H2AX on Lys 5, which is acetylated by Tip60 in response to DNA damage. Furthermore, we showed that Tip60 and Tip60-mediated acetylation of H2AX are required for effective MDC1, BRCA1 and Rad51 foci formation. Overexpression of Sirt1 resulted in repressed H2AX acetylation. In addition, depletion of Sirt1 resulted in accelerated H2AX acetylation, leading to increased foci formation of MDC1, BRCA1 and Rad51. These findings strongly suggested that Sirt1 negatively regulates the formation of these foci after γIR, probably via negatively regulating Tip60-mediated H2AX acetylation on Lys 5.

Interestingly, Sirt1 interacts with Tip60 without DNA damage, and depletion of Sirt1 results in accelerated H2AX acetylation without DNA damage. These results might indicate that Sirt1 aggressively represses excessive H2AX acetylation in response to intrinsic DNA damage.

The mechanism by which acetylated H2AX is regulated by Sirt1

In this report, we showed that Sirt1 stimulates proteasome-dependent degradation of Tip60. This indicates that Sirt1 negatively regulates the level of Tip60 protein *in vivo*. Interestingly, Sirt1 deacetylates acetylated Tip60. Although Tip60 is highly auto-acetylated *in vivo* [20], after γIR, Tip60 is deacetylated gradually, relative to the deacetylase activity of Sirt1. Previous reports have described that a deacetylated form of Foxo3a (Foxo3a is acetylated by p300/CBP and deacetylated by Sirt1) is less stable than the acetylated form [22]. We therefore assumed that auto-acetylation of Tip60 protects Tip60 itself from proteasome-dependent protein degradation, and that Sirt1 stimulates proteasome-dependent protein degradation of Tip60 by removing acetyl group(s) from acetylated lysine residue(s) of Tip60 required for stability. The decrease of Tip60 protein level may result in repression of acetylated H2AX on Lys5. This hypothesis might explain why the deacetylase activity of Sirt1 is required for Tip60 degradation. We cannot exclude the possibility that Sirt1 directly removes an acetyl group from acetylated H2AX. However, this is unlikely, as Sirt1 could not deacetylate acetylated H2AX *in vitro* and this hypothesis cannot explain the physical interaction between Tip60 and Sirt1.

Interestingly, H363YSirt1 also sensitized cells to γIR as well as wild-type Sirt1, although Tip60 could not rescue it. A recent report has shown that Sirt1$^{-/-}$ DT40 cells, which show no defects in cell cycle checkpoint and DNA damage repair, are more susceptible to cell death following γIR than wild-type cells. Thus H363YSirt1 might inhibit functions of Sirt1 other than cell cycle checkpoint and DNA damage repair in a dominant-negative manner, resulting in a defect of cellular viability following γIR [24].

Biological meaning of repressing acetylation of H2AX

The depletion of Sirt1 results in increased foci formation of MDC1, BRCA1, and Rad51, indicating that Sirt1 negatively regulates the formation of these foci after γIR. Because IRIF formation is a critical event for DDR signaling [4], our findings strongly suggest that Sirt1 can suppress the DDR pathway. However, Sirt1-mediated repression of DDR seems to be unfavorable to DNA-damaged cells and inconsistent with the anti-apoptotic function of Sirt1 [25]. Perhaps if Tip60 incorrectly stimulates IRIF formation, IRIF-dependent excessive and/or prolonged activation of DDR signaling might have a negative effect on the survival of cells with DNA damage due to excessive DDR signal-dependent apoptosis. Accordingly, Sirt1 may repress DDR signals by suppressing Tip60 activity. Our results indicated that Sirt1 could not only repress IRIF, but also Rad51 foci formation. This implies that Rad51-dependent HR is negatively regulated by Sirt1 (because HR repair is thought to take place at Rad51 foci, our results may suggest that HR repair can be repressed by Sirt1 [23]). Sirt1 may achieve genomic stability by negatively regulating HR repair, such as BLM, p53, and the mismatch repair system, because excessive HR is deleterious to cells [26]. Inconsistent with this hypothesis, we found that overexpression of Sirt1 results in reduced cellular viability post-γIR, and that Tip60 can rescue the defect. However, we do not think that it is difficult to explain the discrepancy. That is; as shown in Fig. 3, despite a significant amount of Sirt1, deacetylation of Tip60 progressed slowly for some hours after γIR. This phenomenon suggested that deacetylation of Tip60 by Sirt1 is regulated by a DDR-induced mechanism. Such a mechanism would cause Sirt1 to negatively regulate Tip60 at an appropriate time point. In our system, constitutive overexpression of Sirt1 may result in inappropriate inactivation of Tip60, leading to the loss of cellular viability. In budding yeast, ESA1 as well as other HATs are initially recruited to DSB, followed by recruitment of HDACs—including Sir2 (yeast's Sirt1 homolog)—during HR repair [19]. In also mammals, the ordered recruitment of HAT and HDAC to DSB is required for the regulation of the acetylation state of histones around DSB.

Finally, we have shown that acetylation of H2AX at Lys5 is not only positively regulated by Tip60, but also negatively regulated by Sirt1. This complicated regulation of H2AX acetylation may play an important role in DDR.

Funding

This work was supported in part by Grants-in-Aid for Scientific Research from the Ministry of Health, Labor and Welfare and the

Ministry of Education, Culture, Sports, Science and Technology of Japan. Additional support was provided by The Program for Promotion of Fundamental Studies of the National Institute of Biomedical Innovation of Japan.

Conflict of interest statement

None declared.

Acknowledgment

We greatly appreciate the gift of the wild-type and H363Y Sirt1-myc expression vectors from Dr. Tony Kouzarides. LPSX vector was kindly provided by Dr. Hitoshi Ichikawa (NCC, Tokyo). We thank Dr. Misao Ohki for advice and critical comments on the manuscript.

Appendix A. Supplementary data

Supplementary data associated with this article can be found, in the online version, at doi:10.1016/j.bbrc.2009.10.156.

References

[1] J. Rouse, S.P. Jackson, Interfaces between the detection, signaling, and repair of DNA damage, Science 297 (2002) 547–551.
[2] Z. Lou, K. Minter-Dykhouse, S. Franco, et al., MDC1 maintains genomic stability by participating in the amplification of ATM-dependent DNA damage signals, Mol. Cell 21 (2006) 187–200.
[3] T.T. Paull, E.P. Rogakou, V. Yamazaki, et al., A critical role for histone H2AX in recruitment of repair factors to nuclear foci after DNA damage, Curr. Biol. 10 (2000) 886–895.
[4] A. Celeste, O. Fernandez-Capetillo, M.J. Kruhlak, et al., Histone H2AX phosphorylation is dispensable for the initial recognition of DNA breaks, Nat. Cell Biol. 5 (2003) 675–679.
[5] E.P. Rogakou, C. Boon, W.M. Bonner, Mega-base chromatin domains involved in DNA double-strand breaks *in vivo*, J. Cell Biol. 146 (1999) 905–916.
[6] T. Ikura, V.V. Ogryzko, M. Grigoriev, et al., Involvement of the TIP60 histone acetylase complex in DNA repair and apoptosis, Cell 102 (2000) 463–473.
[7] T. Kusch, L. Florens, W.H. MacDonald, et al., Acetylation by Tip60 is required for selective histone variant exchange at DNA lesions, Science 306 (2004) 2084–2087.
[8] S. Pagans, A. Pedal, B.J. North, et al., SIRT1 regulates HIV transcription via Tat deacetylation, PLoS Biol. 3 (2005) 210–220.
[9] R. Murr, J.I. Loizou, Y.G. Yang, et al., Histone acetylation by Trrap-Tip60 modulates loading of repair proteins and repair of DNA double-strand breaks, Nat. Cell Biol. 8 (2006) 91–99.
[10] T. Ikura, S. Tashiro, A. Kakino, et al., DNA damage-dependent acetylation and ubiquitination of H2AX enhances chromatin dynamics, Mol. Cell Biol. 27 (2007) 7028–7040.
[11] A.W. Bird, D.Y. Yu, M.G. Pray-Grant, et al., Acetylation of histone H4 by Esa1 is required for DNA double-strand break repair, Nature 419 (2002) 411–415.
[12] S. Imai, C. Armstrong, M. Kaeberlein, et al., Transcriptional silencing and longevity protein Sir2 is an NAD-dependent histone deacetylase, Nature 403 (2000) 795–800.
[13] J. Luo, A.Y. Nikolaev, S. Imai, et al., Negative control of p53 by Sir2-alpha promotes cell survival under stress, Cell 107 (2001) 137–148.
[14] H. Vaziri, S.K. Dessain, E. Eaton, et al., HSIR2-SIRT1 functions as an NAD-dependent p53 deacetylase, Cell 107 (2001) 149–159.
[15] A. Brunet, L.B. Sweeney, J.F. Sturgrill, et al., Stress-dependent regulation of FOXO transcription factors by the SIRT1 deacetylase, Science 303 (2004) 2011–2015.
[16] H. Cohen, C. Miller, K.J. Bitterman, et al., Calorie restriction promotes mammalian cell survival by inducing the SIRT1 deacetylase, Science 305 (2004) 390–392.
[17] F. Yeung, J.E. Hoberg, C.S. Ramsey, et al., Modulation of NF-kappaB-dependent transcription and cell survival by the SIRT1 deacetylase, EMBO J. 23 (2004) 2369–2380.
[18] Z. Yuan, X. Zhang, N. Sengupta, et al., SIRT1 regulates the function of the Nijmegen breakage syndrome protein, Mol. Cell 27 (2007) 149–162.
[19] B.A. Tamburini, J.K. Tyler, Localized histone acetylation and deacetylation triggered by the homologous recombination pathway of double-strand DNA repair, Mol. Cell Biol. 25 (2005) 4903–4913.
[20] Y. Tang, J. Luo, W. Zhang, et al., Tip60-dependent acetylation of p53 modulates the decision between cell-cycle arrest and apoptosis, Mol. Cell 24 (2006) 827–839.
[21] E. Col, C. Caron, C. Chable-Bessia, G. Legube, et al., HIV-1 tat targets Tip60 to impair the apoptotic cell response to genotoxic stresses, EMBO J. 24 (2005) 2634–2645.
[22] M.C. Motta, N. Divecha, M. Lemieux, et al., Mammalian SIRT1 represses forkhead transcription factors, Cell 116 (2004) 551–563.
[23] M.K. Shivji, A.R. Venkitaraman, DNA recombination, chromosomal stability and carcinogenesis: insights into the role of BRCA2, DNA Repair (Amst.) 3 (2004) 835–843.
[24] N. Matsushita, Y. Takami, M. Kimura, et al., Role of NAD-dependent deacetylases SIRT1 and SIRT2 in radiation and cisplatin-induced cell death in vertebrate cells, Genes Cells 10 (2005) 321–332.
[25] M.E. Giannakou, L. Partridge, The interaction between FOXO and SIRT1: tipping the balance towards survival, Trends Cell Biol. 14 (2004) 408–412.
[26] P. Bertrand, Y. Saintigny, S.B. Lopez, P53's double life: transactivation-independent repression of homologous recombination, Trends Genet. 20 (2004) 235–243.

Indispensable Role of the Runx1-Cbfβ Transcription Complex for In Vivo-Suppressive Function of FoxP3$^+$ Regulatory T Cells

Akihiko Kitoh,[1,2] Masahiro Ono,[1,2,3] Yoshinori Naoe,[4] Naganari Ohkura,[1,3,5] Tomoyuki Yamaguchi,[1] Hiroko Yaguchi,[1,3,5] Issay Kitabayashi,[6] Toshihiko Tsukada,[5] Takashi Nomura,[1] Yoshiki Miyachi,[2] Ichiro Taniuchi,[4] and Shimon Sakaguchi[1,3,*]
[1]Department of Experimental Pathology, Institute for Frontier Medical Sciences
[2]Department of Dermatology
Graduate School of Medicine, Kyoto University, Kyoto 606-8507, Japan
[3]Laboratory of Experimental Immunology, WPI Immunology Frontier Research Center, Osaka University, Suita 565-0871, Japan
[4]Laboratory for Transcriptional Regulation, RIKEN Research Center for Allergy and Immunology, Kanagawa 230-0045, Japan
[5]Tumor Endocrinology Project
[6]Molecular Oncology Division
National Cancer Center Research Institute, Tokyo 104-0045, Japan
*Correspondence: shimon@frontier.kyoto-u.ac.jp
DOI 10.1016/j.immuni.2009.09.003

SUMMARY

Naturally arising regulatory T (Treg) cells express the transcription factor FoxP3, which critically controls the development and function of Treg cells. FoxP3 interacts with another transcription factor Runx1 (also known as AML1). Here, we showed that Treg cell-specific deficiency of Cbfβ, a cofactor for all Runx proteins, or that of Runx1, but not Runx3, induced lymphoproliferation, autoimmune disease, and hyperproduction of IgE. *Cbfb*-deleted Treg cells exhibited impaired suppressive function in vitro and in vivo, with altered gene expression profiles including attenuated expression of FoxP3 and high expression of interleukin-4. The Runx complex bound to more than 3000 gene loci in Treg cells, including the *Foxp3* regulatory regions and the *Il4* silencer. In addition, knockdown of *RUNX1* showed that RUNX1 is required for the optimal regulation of FoxP3 expression in human T cells. Taken together, our results indicate that the Runx1-Cbfβ heterodimer is indispensable for in vivo Treg cell function, in particular, suppressive activity and optimal expression of FoxP3.

INTRODUCTION

CD4$^+$CD25$^+$FoxP3$^+$ naturally occurring regulatory T (Treg) cells play essential roles for the maintenance of immunological self-tolerance and immune homeostasis by actively suppressing aberrant or excessive immune responses harmful to the host (Sakaguchi et al., 2006). Natural Treg cells specifically express the transcription factor FoxP3, which critically controls the development and the function of Treg cells as illustrated by *FOXP3* mutations (Ochs et al., 2005). FoxP3 deficiency or dysfunction in humans results in the development of IPEX (immune dysregulation, polyendocrinopathy, enteropathy, X-linked) syndrome, which is characterized by severe autoimmune disease, allergy, and inflammatory bowel disease (Sakaguchi et al., 2006). FoxP3 expression can confer suppressive activity to Treg cells, suppress the production of cytokines such as interleukin-2 (IL-2) and interferon-gamma (IFN-γ), and upregulate the expression of Treg cell-associated molecules including CD25 and cytotoxic T lymphocyte-associated antigen 4 (CTLA-4) (Fontenot et al., 2003; Hori et al., 2003; Khattri et al., 2003). Recent studies have shown that the gene regulatory function of FoxP3 requires its association with other transcription factors, such as NFAT (nuclear factor of activated T cells), NF-κB (nuclear factor-κB), and Runx1 (runt-related transcription factor 1), also known as AML1 (acute myeloid leukemia 1), and with histone deacetylases and acetyltransferases (Bettelli et al., 2005; Li et al., 2007; Ono et al., 2007; Wu et al., 2006). Yet, the precise molecular mechanisms by which FoxP3 controls Treg cell function remain to be elucidated.

The Runx (AML) transcription factors consist of three members: Runx1 (AML1), Runx2 (AML3), and Runx3 (AML2) (van Wijnen et al., 2004). All Runx proteins bind to the specific DNA consensus sequences (ACCACA) via a highly conserved DNA-binding *runt* domain. Runx binding is stabilized by the association with Cbfβ (core-binding factor β), a non-DNA-binding cofactor essential for the function of all Runx proteins (Speck, 2001). The Runx-Cbfβ heterodimeric complex interacts with other DNA-binding transcription factors, coactivators, or corepressors to either activate or repress expression of the target genes in a context-dependent manner (Durst and Hiebert, 2004; Taniuchi and Littman, 2004). In addition to the essential requirement of Runx proteins for definitive hematopoiesis (de Bruijn and Speck, 2004), Runx1 and Runx3 are crucially involved in the differentiation and function of peripheral T cells (Djuretic et al., 2007; Komine et al., 2003; Naoe et al., 2007; Zhang et al., 2008) as well as thymic T cell development (Grueter et al., 2005; Sato et al., 2005; Setoguchi et al., 2008; Taniuchi et al., 2002; Woolf et al., 2003). We have previously shown that Runx1 binds to the promoter of the *Il2* and *Ifng* genes and upregulates the production of IL-2 and IFN-γ, respectively. Further, FoxP3 binds to Runx1 in Treg cells, thereby repressing *Il2* and *Ifng* and

activating the genes encoding CD25 (*Il2ra*) and CTLA-4 (*Ctla4*) (Ono et al., 2007). We have also shown that, in vitro, FoxP3 can interact with the other members of the Runx family, Runx2 and Runx3, in addition to Runx1 (Ono et al., 2007). These findings collectively suggest that the Runx-dependent transcription program operating in conventional T cells could be modulated in Treg cells through interaction with FoxP3. Yet, it remains obscure whether the Runx-mediated gene regulation is indeed required for the in vivo function of Treg cells.

In this report, we have generated mice with Treg cell-specific conditional deletion of *Cbfb* to analyze in vivo the possible contribution of Runx-dependent gene regulation to Treg cell function because all Runx proteins need to form a heterodimeric complex with Cbfβ for exerting transcriptinal activities and Cbfβ deficiency disrupts the function of the Runx complex (Speck, 2001). Here, we showed that Treg cell-specific Cbfβ-deficient mice spontaneously developed lymphoproliferation, autoimmune disease, and IgE hyperproduction and that *Cbfb*-deleted Treg cells exhibited impaired suppressive activity both in vitro and in vivo. In addition, Treg cell-specific conditional deletion of *Runx1*, but not *Runx3*, led to the development of immunological diseases similar to those observed in Treg cell-specific Cbfβ deficiency. Our findings thus indicate that the heterodimeric Runx1-Cbfβ complex is an indispensable transcription regulator for in vivo functions of Treg cells and that it is a potential therapeutic target for controlling physiological and pathological immune responses.

RESULTS

Treg Cell-Specific Deletion of *Cbfb* and the Resulting Development of Autoimmune Disease

To determine whether Runx proteins were required for in vivo function of FoxP3$^+$ Treg cells, we generated Treg cell-specific *Cbfb*-deleted mice by crossing mice harboring *LoxP*-flanked *Cbfb* allele with *Foxp3-Ires-Cre* (*FIC*) knockin mice, which faithfully express Cre recombinase in FoxP3$^+$ T cells (Naoe et al., 2007; Wing et al., 2008). FIC-mediated genomic deletion of *LoxP*-flanked region occurred in almost 100% CD4$^+$FoxP3$^+$ cells and a small population of CD8$^+$ T cells (Wing et al., 2008). With genomic DNA-PCR analyses of subpopulations of thymocytes and splenic T cells from *Cbfb$^{F/F}$: FIC* mice, inactivation of the *Cbfb* gene was initiated specifically in CD4-single positive (CD4SP) HSA^{lo}CD25^{hi} mature thymocytes and was completed in CD4$^+$CD25^{hi} splenic T cells, indicating Treg cell-specific deletion of the *Cbfb* gene (Figure 1A, left). Some of the CD4$^+$CD25$^-$ T cells also harbored the genomic *Cbfb* deletion (Figure 1A, left). This can be attributed to the presence of CD4$^+$CD25$^-$FoxP3$^+$ Treg cells in this CD4$^+$CD25$^-$ population (Figure S1 and Supplemental Data available online). As a consequence of the gene inactivation, the Cbfβ protein was undetectable in CD4$^+$CD25^{hi} splenocytes, although a substantial amount of the Cbfβ protein remained in CD4SP HSA^{lo}CD25^{hi} thymocytes (Figure 1A, right). Thus, the Cbfβ protein is gradually decreased in FoxP3$^+$ cells after *Cbfb* gene deletion in the thymus and almost completely lost in the periphery, which is consistent with a similar finding with conditional *Cbfb* deletion by *Cd4-Cre* transgene (Naoe et al., 2007).

Notably, *Cbfb$^{F/F}$: FIC* mice spontaneously developed severe lymphadenopathy and splenomegaly with significantly increased numbers of splenocytes by 14 weeks of age (Figure 1B). Various types of immune cells including CD4$^+$ T cells, CD8$^+$ T cells, B cells, macrophages, and dendritic cells increased in the enlarged spleens of *Cbfb$^{F/F}$: FIC* mice (Figure S2). Seventy percent of *Cbfb$^{F/F}$: FIC* mice developed histologically evident gastritis accompanying high titers of anti-gastric parietal cell autoantibodies in the sera, whereas control *Cbfb$^{F/+}$: FIC* littermates did not (Figures 1C and 1D). Flow cytometric analysis revealed that non-Treg T cells, i.e., CD4$^+$FoxP3$^-$ conventional T cells and CD8$^+$ T cells, in *Cbfb$^{F/F}$: FIC* mice showed an activated or memory phenotype; e.g., CD69$^+$, CD122$^+$, CD44^{hi}, and CD62L^{lo} (Figure 1E). CD4$^+$ and CD8$^+$ T cells abundantly produced cytokines such as IFN-γ, IL-2, IL-4, and IL-10, as revealed by intracellular cytokine staining after stimulation with PMA and ionomycin (Figure 1F). In addition, *Cbfb$^{F/F}$: FIC* mice showed 10-fold elevated concentrations of serum IgE and 1.5-fold increase in serum IgG (Figure 1G). Thus, Treg cell-specific Cbfβ deficiency produced autoimmune disease and led to hyperproduction of IgE.

The Effects of Treg Cell-Specific *Cbfb* Gene Deletion on Treg Cell Development and Function

To analyze the mechanism of autoimmunity caused by Treg cell-specific *Cbfb* deficiency, we attempted to determine whether thymic generation and differentiation of Treg cells, their peripheral survival, or their suppressive function was affected by the deficiency.

There was no significant difference in the number of total or FoxP3$^+$ thymocytes between *Cbfb$^{F/F}$: FIC* and *Cbfb$^{F/+}$: FIC* mice (Figure 2A and Figure S3). HSA^{lo}CD25^{hi}FoxP3$^+$CD4SP thymic Treg cells normally developed in *Cbfb$^{F/F}$: FIC* mice as in control *Cbfb$^{F/+}$: FIC* mice (Figure 2B). Whereas Runx proteins were required for the differentiation of immature thymocytes to TCRβ^{hi}HSA^{lo}CD4SP mature thymocytes (Egawa et al., 2007), the generation of FoxP3$^+$TCRβ^{hi}HSA^{lo}CD4SP mature thymocytes was not markedly impaired in *Cbfb$^{F/F}$: FIC* mice (Figure S4). Residual Cbfβ protein might be sufficient to support differentiation and maturation of FoxP3$^+$ cells in the thymus (Figure 1A).

We next examined whether Treg cell homeostasis was impaired in the periphery of *Cbfb*-deleted mice. The proportion of CD4$^+$FoxP3$^+$ Treg cells to total CD4$^+$ T cells and the absolute number of Treg cells were slightly higher in *Cbfb$^{F/F}$: FIC* mice than in *Cbfb$^{F/+}$: FIC* mice (Figures 2C and 2D). Notably, Treg cells in *Cbfb$^{F/F}$: FIC* mice showed substantially decreased expression of FoxP3, compared to those in control mice (Figure 2D). Expression of Ki-67, a cellular marker for proliferation, indicated that an equivalent or larger proportion of Treg cells were active in cell cycle in *Cbfb$^{F/F}$: FIC* mice compared with control mice (Figure 2E). In *Cbfb$^{F/F}$: FIC* mice, Ki-67$^-$ resting Treg cells showed reduced expression of FoxP3, whereas Ki-67^{hi} proliferating Treg cells expressed FoxP3 at equivalent amounts as Ki-67^{hi} Treg cells in control mice (Figure 2E). In vivo BrdU labeling also revealed that CD4$^+$CD25^{hi} splenocytes in *Cbfb$^{F/F}$: FIC* mice were more actively proliferating than those in *Cbfb$^{F/+}$: FIC* mice (Figure 2F). Treg cells in the former expressed only slightly lower amounts of CD127 (IL-7 receptor α chain) and were not apoptotic according to 7-AAD (7-amino-actinomycin D) and Annexin V staining, in accord with the previous finding that *Runx1*-deficient

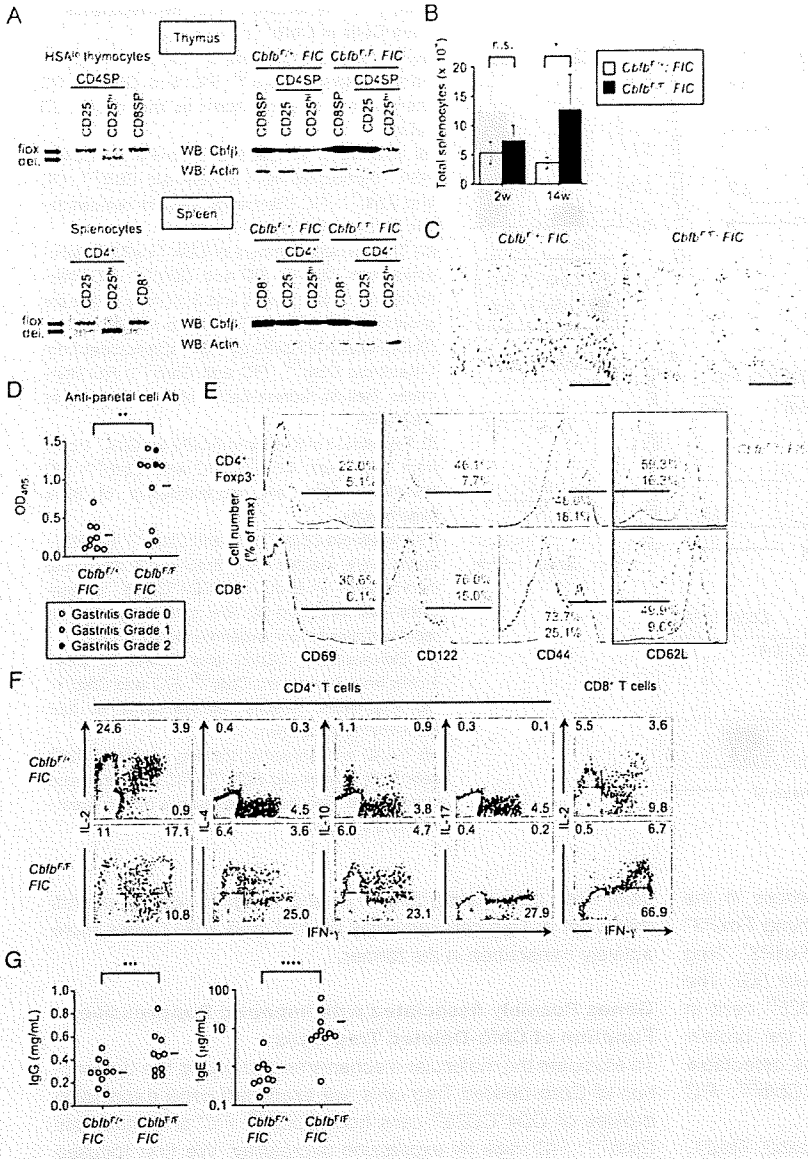

Figure 1. Treg Cell-Specific *Cbfb* Deficiency Induced Autoimmune Disease and Hyperproduction of IgE

(A) Treg cell-specific *Cbfb* deletion in *Cbfb*$^{F/F}$*: FIC* mice. PCR analysis (left) for detecting *Cbfb*^{F} (flox) and *Cbfb*-deleted (del.) alleles of the *Cbfb* gene was performed with genomic DNA from indicated thymocyte (top) and splenocyte (bottom) subpopulations of *Cbfb*$^{F/F}$*: FIC* mice as templates. Immunoblot analysis (right) of Cbfβ protein expression in indicated thymocyte (top) and splenocyte (bottom) subpopulations of *Cbfb*$^{F/F}$*: FIC* and control *Cbfb*$^{F/+}$*: FIC* littermates is shown. Results representative of two experiments are shown.

(B) The absolute numbers of total splenocytes are shown as the mean ± SD value from *Cbfb*$^{F/F}$*: FIC* mice and *Cbfb*$^{F/+}$*: FIC* littermates (n = 4) at 2 and 14 weeks of age. *p = 0.02.

(C) Hematoxylin and eosin staining of sections from stomachs of 7- to 8-week-old *Cbfb*$^{F/F}$*: FIC* and *Cbfb*$^{F/+}$*: FIC* littermates (n = 10). Representative photomicrographs are shown. Scale bars represent 10.0 μm.

(D) Titers of parietal cell autoantibodies in the sera of 8-week-old *Cbfb*$^{F/F}$*: FIC* and *Cbfβ*$^{F/+}$*: FIC* littermates (n = 10) were assessed by ELISA. Horizontal lines represent averages from each group. **p = 0.01.

(E) Activated surface-marker phenotype of CD4$^+$FoxP3$^-$ conventional T cells and CD8$^+$ T cells in *Cbfb*$^{F/F}$*: FIC* mice at 16 weeks of age. Data are representative of five experiments.

(F) Production of proinflammatory cytokines by CD4$^+$ and CD8$^+$ T cells in *Cbfb*$^{F/F}$*: FIC* mice at 14 weeks of age. Data are representative of three experiments.

(G) Titers of IgG and IgE in the sera of 8-week-old *Cbfb*$^{F/F}$*: FIC* and *Cbfb*$^{F/+}$*: FIC* littermates (n = 10) were assessed by ELISA. Horizontal lines represent averages from each group. ***p = 0.04; ****p = 0.001.

Treg cells in *Runx1*$^{F/F}$*: Cd4-Cre* mice were apoptosis resistant (Egawa et al., 2007) (Figures 2G and 2H).

Phenotypically, *Cbfb*-deleted Treg cells expressed CD25 and glucocorticoid-induced tumor necrosis factor receptor family-related protein (GITR) at higher amounts and CTLA-4 at equivalent amounts compared to control Treg cells, whereas they scarcely expressed CD103 in accord with the finding that Runx3 controls CD103 expression (Grueter et al., 2005) (Figure 3A). Neither *Cbfb*-deleted nor control Treg cells proliferated in response to in vitro polyclonal TCR stimulation with anti-CD3 (Figure 3B). Yet, *Cbfb*-deleted Treg cells were less suppressive in vitro (Figure 3C). In addition, they failed to prevent the development of colitis and weight loss in SCID mice when cotransferred with BALB/c CD4$^+$CD25$^-$CD45RB^{hi} T cells, in contrast to effective disease prevention by cotransfer of control Treg cells (Figures 3D–3F). Similarly, *Cbfb*-deleted Treg cells failed to suppress the development of gastritis (data not shown). *Cbfb*-deleted Treg cells survived when transferred to SCID mice (Figure S5A), indicating that the impaired in vivo suppressive activity of *Cbfb*-deleted Treg cells was not due to their shorter survival. In addition, the attenuated CD103 expression in *Cbfb*-deleted Treg cells (Figure S5B) would not be responsible for the impaired Treg cell function because others reported that Treg cell-mediated control of colitis did not require CD103 expression by Treg cells (Annacker et al., 2005).

Collectively, these findings indicate that failure in Treg cell-mediated self-tolerance in *Cbfb*$^{F/F}$*: FIC* mice is not due to numerical deficiency, reduced proliferation, or enhanced apoptosis of FoxP3$^+$ Treg cells, but due to their impaired suppressive activity.

Cbfb-Deleted Treg Cells Show Hyperproduction of IL-4

Treg cells hardly produce cytokines such as IL-2, IFN-γ, and IL-4 (Sakaguchi et al., 2006). Flow cytometric analysis revealed that a larger proportion of FoxP3$^+$ Treg cells from *Cbfb*$^{F/F}$*: FIC* mice produced IL-4 and IL-10 compared to Treg cells from control

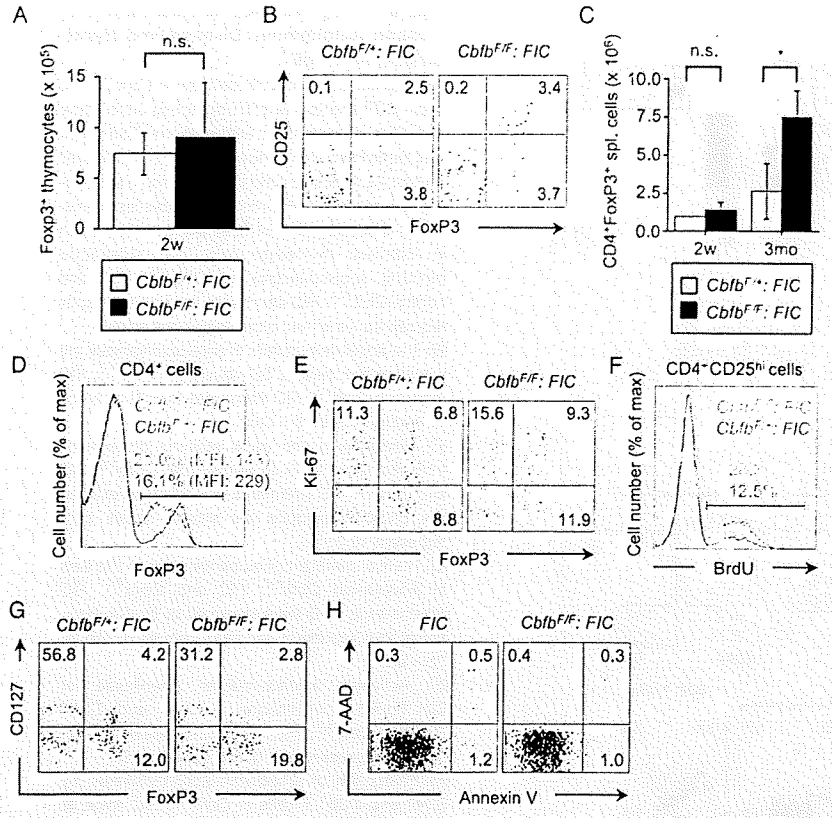

Figure 2. Generation and Homeostasis of Treg Cells in *Cbfb*$^{F/F}$*: FIC* Mice

(A) The absolute numbers of FoxP3$^+$ thymocytes from 2-week-old *Cbfb*$^{F/F}$*: FIC* and *Cbfb*$^{F/+}$*: FIC* littermates (n = 3) are shown as the mean ± SD value.

(B) Expression of CD25 and FoxP3 by CD4SP HSA^{lo} thymocytes from 3-week-old *Cbfb*$^{F/F}$*: FIC* and *Cbfb*$^{F/+}$*: FIC* littermates. Results representative of three experiments are shown.

(C) The absolute numbers of CD4$^+$FoxP3$^+$ splenocytes from *Cbfb*$^{F/F}$*: FIC* and *Cbfb*$^{F/+}$*: FIC* littermates (n = 3) at 2 weeks and 3 months of age are shown as the mean ± SD value. *p = 0.05.

(D) Expression of FoxP3 by CD4$^+$ splenocytes from 7-week-old *Cbfb*$^{F/F}$*: FIC* and *Cbfb*$^{F/+}$*: FIC* littermates. Results representative of five experiments are shown.

(E) Expression of Ki-67 and FoxP3 by CD4$^+$ T cells from 7-week-old *Cbfb*$^{F/F}$*: FIC* and *Cbfb*$^{F/+}$*: FIC* littermates. Data are representative of three experiments.

(F) 9-week-old *Cbfb*$^{F/F}$*: FIC* and *Cbfb*$^{F/+}$*: FIC* littermates were injected with BrdU for 3 days, and incorporation of BrdU into CD4$^+$CD25^{hi} splenocytes was assessed by flow cytometry. Results representative of four experiments are shown.

(G) Expression of CD127 and FoxP3 by CD4$^+$ T cells from 7-week-old *Cbfb*$^{F/F}$*: FIC* and *Cbfb*$^{F/+}$*: FIC* littermates. Results representative of four experiments are shown.

(H) 7-AAD and AnnexinV staining of CD4$^+$CD25^{hi} cells from 8-week-old *Cbfb*$^{F/F}$*: FIC* and littermate control mice. Results representative of two experiments are shown.

mice, whereas there were no substantial differences in the percentage of IL-2- or IFN-γ-producing cells among FoxP3$^+$ Treg cells (Figure 3G). Few IL-17-expressing FoxP3$^+$ Treg cells were present in both groups of mice (Figure 3G). The amount of mRNA for each cytokine in CD4$^+$CD25^{hi} cells in *Cbfb*$^{F/F}$*: FIC* and control mice correlated with the protein expression. However, mRNA for IL-17, which was detectable in *Cbfb*$^{F/+}$*: FIC* mice, was substantially lower in *Cbfb*$^{F/F}$*: FIC* mice (Figure 3H).

Next, the expression of transcription factors *Foxp3*, *Tbx21*, *Gata3*, and *Rorgt*, all of which are essential for Th or Treg cell lineage differentiation, were examined in *Cbfb*-deleted Treg cells. *Foxp3* mRNA expression decreased in *Cbfb*-deleted Treg cells, which is consistent with decreased FoxP3 expression at the protein level (Figure S6). In contrast to the hyperproduction of Th2 cell cytokines IL-4 and IL-10, mRNA expression of Th2 cell-specific transcription factor *Gata3* in *Cbfb*-deleted Treg cells was equivalent to that in control Treg cells, whereas *Cbfb*-deleted Treg cells showed higher expression of Th1 cell-specific transcription factor *Tbx21*. Thus, hyperproduction of Th2 cell cytokines by *Cbfb*-deleted Treg cells was not due to overexpression of *Gata3*, although it has been reported that Runx1 represses *Gata3* expression in conventional CD4$^+$ T cells (Komine et al., 2003). The expression of *Rorgt*, which controls the differentiation of IL-17-producing Th17 cells, also decreased in *Cbfb*-deleted Treg cells compared with control Treg cells (Figure S6). Taken together, our findings show that Cbfβ-deficient Treg cells transcribed *Il17a* and *Rorgt* to lesser extents than control Treg cells, whereas *Il4*, *Il10*, and *Tbx21* were more actively transcribed in the former.

Genes Possibly Associated with Impaired Suppressive Function of *Cbfb*-Deleted Treg Cells

To elucidate the molecular mechanisms underlying the dysfunction of *Cbfb*-deleted Treg cells, we examined gene expression profiles of CD4$^+$CD25^{hi} cells from *Cbfb*$^{F/F}$*: FIC* and littermate *Cbfb*$^{F/+}$*: FIC* mice by expression microarray. We first focused on the previously described "Treg cell signature" genes, which are differentially expressed between Treg cells and conventional CD4$^+$ T cells and therefore thought to be closely related to Treg cell-intrinsic properties including suppressive function (Hill et al., 2007). Sixty-nine signature genes including *Socs2* and *Nrp1* were found to be differentially expressed in *Cbfb*-deleted Treg cells (unpaired t test, $p < 0.05$. see Table S1). Yet, there were not significant differences in the expression of many well-known Treg cell-associated genes, such as *Ctla4*, *Tnfrsf18* (*Gitr*), *Gzmb*, *Folr4*, and *Gpr83*, between *Cbfb*-deleted and control Treg cells (Figure 4A). Decreased mRNA expression of *Itgae* (*CD103*) in *Cbfb*-deleted Treg cells was consistent with the aforementioned flow cytometry results (Figure 4A and Figure 3A). Using the false discovery rate (FDR)-controlling procedure (FDR < 0.2), we further attempted to determine other genes that were differentially expressed in *Cbfb*-deleted Treg cells. We found that 22 and 24 genes were significantly up- or

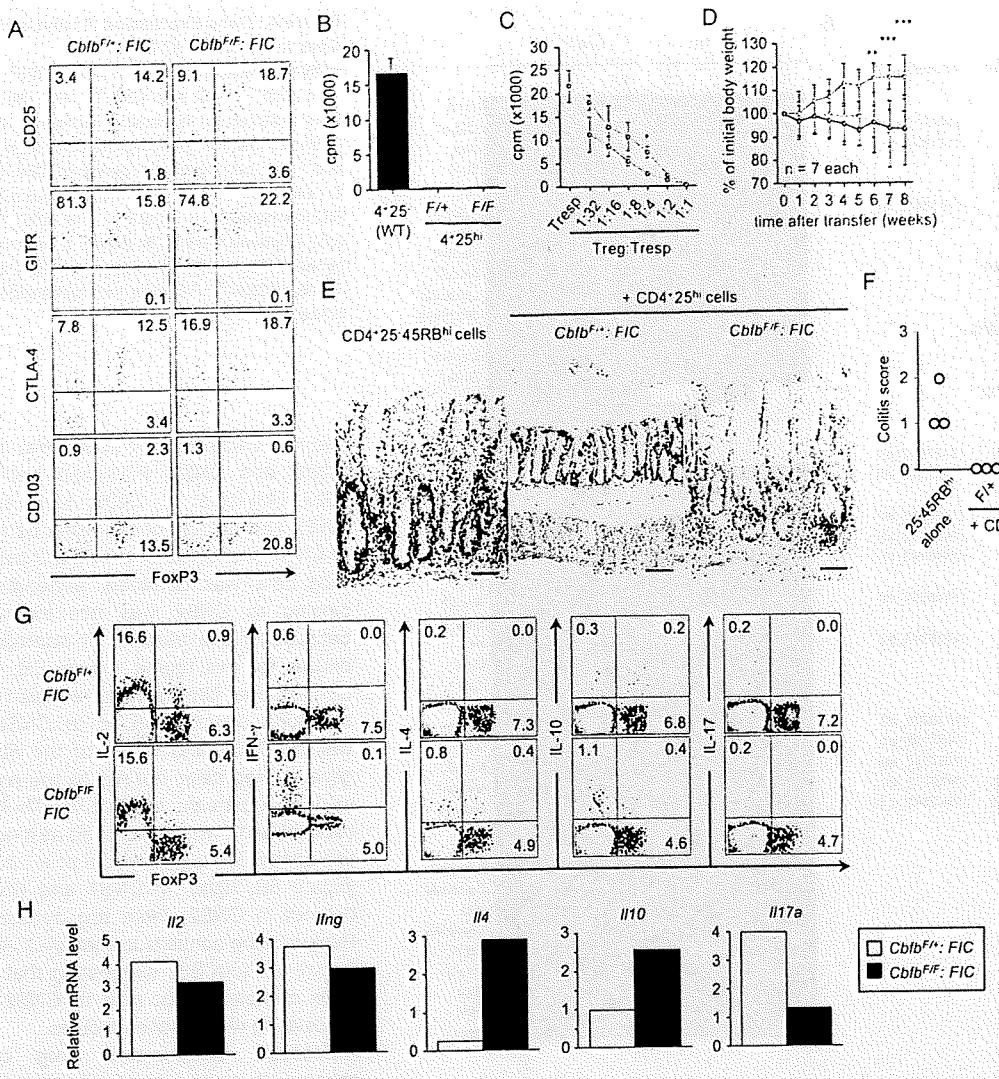

Figure 3. Impaired In Vivo- and In Vitro-Suppressive Activity of *Cbfb*-Deleted Treg Cells

(A) Expression of FoxP3 and other Treg cell-associated molecules by $CD4^+$ T cells from 7-week-old *Cbfb*$^{F/F}$*: FIC* and *Cbfb*$^{F/+}$*: FIC* littermates. Results representative of at least three experiments are shown.

(B) $CD4^+CD25^-$ conventional T cells from wild-type BALB/c mice and $CD4^+CD25^{hi}$ cells from *Cbfb*$^{F/F}$*: FIC* and *Cbfb*$^{F/+}$*: FIC* littermates were stimulated in vitro for 3 days, and cell proliferation was assessed by thymidine incorporation. Data are mean ± SD of triplicates done in one experiment representative of seven.

(C) In vitro suppression assay with $CD4^+CD25^-$ T cells from 6-week-old wild-type BALB/c mice as responders and $CD4^+CD25^{hi}$ T cells from 5-week-old *Cbfb*$^{F/F}$*: FIC* (red lines) or *Cbfb*$^{F/+}$*: FIC* (blue lines) littermates as suppressors. Data are mean ± SD of triplicates done in one experiment representative of four. $^*p = 0.004$ (unpaired t test).

(D) Eight-week-old C.B-17 SCID mice received 4×10^5 $CD4^+CD25^-CD45RB^{hi}$ cells purified from wild-type BALB/c mice either alone (black lines) or together with 3×10^5 $CD4^+CD25^{hi}$ cells purified from 6-week-old *Cbfb*$^{F/F}$*: FIC* (red lines) or *Cbfb*$^{F/+}$*: FIC* (blue lines) littermates. Body weight is represented as the percentage of initial weight (mean ± SD). Results from a total of four independent experiments are shown. $^{**}p = 0.01$; $^{***}p = 0.02$, *Cbfb*$^{F/F}$*: FIC* versus *Cbfb*$^{F/+}$*: FIC* by Mann-Whitney U test.

(E) Hematoxylin and eosin staining of sections from colons of SCID mice transferred as described in (D) (n = 3 each group). Representative photomicrographs are shown. Scale bars represent 10.0 μm.

(F) Colitis were histologically scored (n = 3 each group).

(G) Costaining of FoxP3 and the indicated cytokines in $CD4^+$ T cells from 14-week-old *Cbfb*$^{F/F}$*: FIC* and *Cbfb*$^{F/+}$*: FIC* littermates fter the stimulation with PMA and ionomycin for 6 hr. Results representative of three experiments are shown.

(H) Relative mRNA expression of the indicated cytokines in $CD4^+CD25^{hi}$ cells purified from *Cbfb*$^{F/F}$*: FIC* and *Cbfb*$^{F/+}$*: FIC* littermates at 6 weeks of age. Data are representative of two experiments.

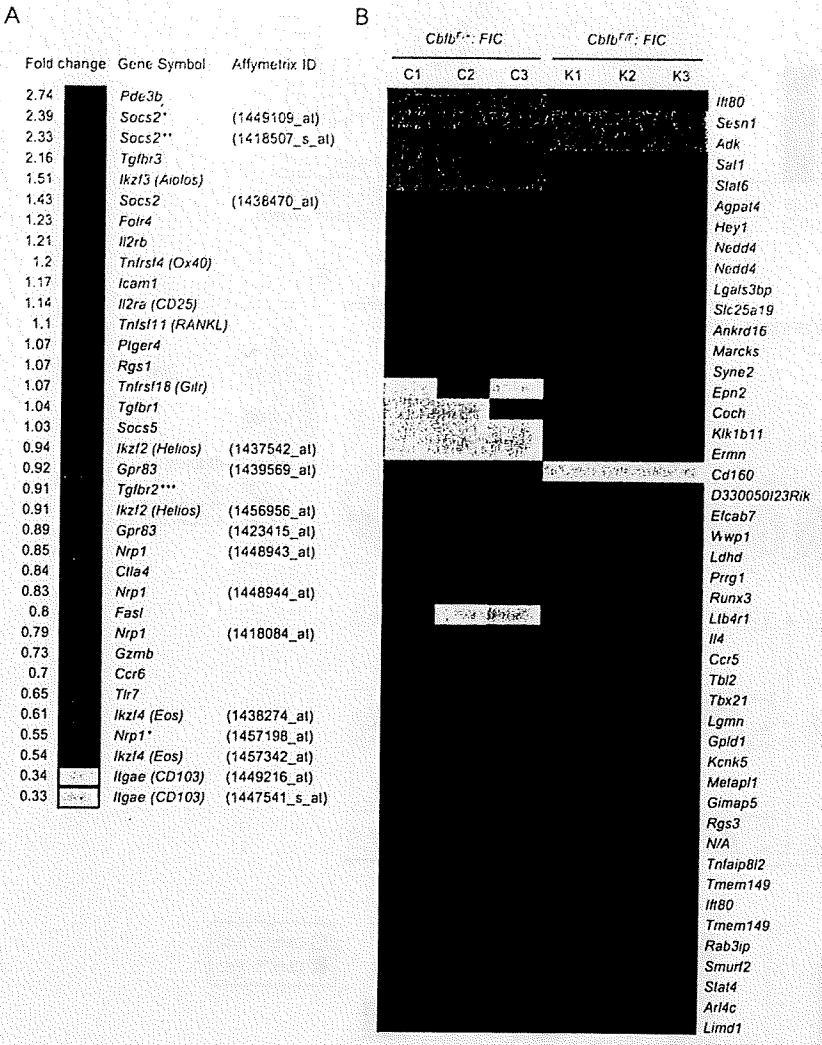

Figure 4. Gene Expression Analysis of Treg Cells in *Cbfb*$^{F/F}$*: FIC* Mice

mRNA expression profiles of CD4$^+$CD25^h T cells from *Cbfb*$^{F/F}$*: FIC* and *Cbfb*$^{F/+}$*: FIC* littermates were analyzed by expression microarray (n = 3). (A) shows fold change in expression of representative "Treg cell signature" genes in CD4$^+$CD25^h T cells from *Cbfb*$^{F/F}$*: FIC* mice versus *Cbfb*$^{F/+}$*: FIC* littermates. *, p = 0.01; **, p = 0.03; ***, p = 0.02 (unpaired t test). (B) shows a heat map of genes differentially expressed in CD4$^+$CD25^h T cells of *Cbfb*$^{F/F}$*: FIC* mice with statistical significance (FDR < 0.2).

downregulated, respectively, in *Cbfb*-deleted Treg cells (Figure 4B and Table S2). Differentially expressed molecules included IL-4, CCR5, leukotriene B4 receptor 1 (Ltb4r1, also called BLT1), and CD160, which are secreted or have extracellular regions possibly involved in cellular interactions.

The Runx Complex Binds to the Regulatory Regions of Many Genes Including *Foxp3* and *Il4*

To further investigate Runx-dependent gene regulation in Treg cells, we attempted to identify target genes of the Runx complex. Genome-wide analysis with chromatin immunoprecipitation (ChIP) coupled with promoter tiling array showed that the Runx complex bound to the promoter regions of 3566 genes including *Foxp3* (Figure 5A and Table S3). Similar analysis with the customized array covering the *Foxp3* gene locus revealed that the Runx complex bound to several regions of the *Foxp3* gene in Treg cells prepared from wild-type BALB/c mice (Figure 5B, left). It has been reported that the following three conserved noncoding sequences (CNSs) contribute to *Foxp3* expression: one CNS located in 0.5 kb upstream of the transcription start site (CNS1) and two CNSs located in the first intron (CNS2 and CNS3) (Kim and Leonard, 2007; Mantel et al., 2006; Tone et al., 2008). The binding of the Runx complex to CNS1 and CNS3 of the *Foxp3* gene in Treg cells was detected, although the binding to CNS2 was not examined because of unavailability of appropriate probes for this region (Figure 5B, left). Conventional ChIP assays revealed that the Runx complex bound to CNS2 as well as CNS1 and CNS3 of the *Foxp3* gene in Treg cells, but not to the region at 1 kb upstream of *Zbtb7b* (*Th-POK*) exon Ia (UP1), which was used as a negative control locus (Setoguchi et al., 2008) (Figure 5B, right). In CNS1 and CNS3, but not in CNS2, there are conserved Runx-binding consensus sites (ACCACA) (Figure S7 and S8), suggesting that the Runx complex might bind to CNS2 via associating with other molecules.

Because *Cbfb*-deleted Treg cells showed IL-4 hyperproduction without overexpression of *Gata3*, we investigated how the Runx complex controlled *Il4* expression in Treg cells. By promoter tiling array analysis, we could not detect the binding of the Runx complex to the *Il4* promoter region in Treg cells. However, by coupling ChIP assay with custom tiling array for the Th2 cytokine locus (~200 base intervals), we found that the Runx complex bound to the *Il4* silencer in Treg cells (Figure 5C, left). We further confirmed this binding by conventional ChIP assays (Figure 5C, right). Thus, the Runx complex may repress *Il4* expression in Treg cells via binding to the *Il4* silencer as in naive CD4$^+$ T cells and Th1 cells, as we and others have recently reported (Djuretic et al., 2007; Naoe et al., 2007). ChIP and promoter tiling array also revealed that the Runx complex bound to the promoter region of the *Ifng* gene in Treg cells, being consistent with our previous finding that Runx1 bound to this region (Ono et al., 2007) (Figure S9). The Runx complex also bound to the regulatory region of the *Gzmb* gene, which is highly expressed in Treg cells in specific environment and is involved in Treg cell-suppressive function (Cao et al., 2007; Gondek et al., 2005) (Figure S10). Thus, the Runx complex binds

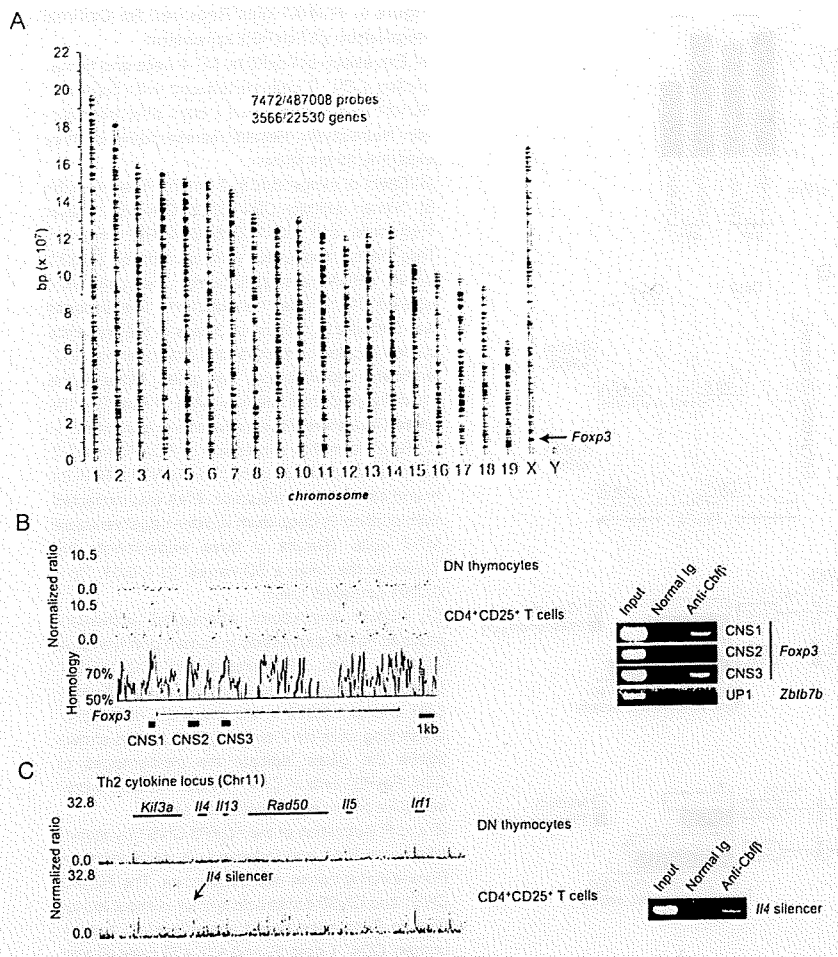

Figure 5. Binding of the Runx Complex to Regulatory Regions of *Foxp3* and *Il4*

(A) The Runx complex bound to promoter regions of various genes in Treg cells. MACS-purified $CD4^+CD25^+$ T cells of wild-type BALB/c mice were subjected to ChIP with anti-Cbfβ followed by promoter tiling array. Red crosses indicate Cbfβ-bound genes.

(B) The Runx complex bound to CNSs of the *Foxp3* gene in Treg cells of BALB/c mice. The binding of the Runx complex to the *Foxp3* gene locus in double negative (DN) thymocytes and peripheral $CD4^+CD25^+$ T cells from BALB/c mice was examined through a custom tiling array for the *Foxp3* locus coupled with ChIP with Cbfβ antibody (left). The signal intensity value of an individual probe is represented by a red dot in correspondence to the structure of the mouse *Foxp3* gene and mouse-human VISTA homology plot of the *Foxp3* gene. Red areas and blue areas in the VISTA plot indicate highly homologous regions and the exons of the mouse *Foxp3* gene, respectively. Gray squares in the figure of *Foxp3* gene structure indicate 5′ untranslated regions (UTRs). The binding of the Runx complex to CNSs of the *Foxp3* gene and the UP1 region of the *Zbtb7b* gene was assessed by conventional ChIP assays (right).

(C) The Runx complex bound to the *Il4* silencer in Treg cells of BALB/c mice. The binding of the Runx complex to the *Il4* silencer in $CD4^+CD25^+$ T cells from BALB/c mice was detected with the combination of ChIP and genome tiling array customized for Th2 cytokine locus (left) and conventional ChIP assays (right).

to the regulatory regions of *Foxp3*, *Il4*, and other genes in Treg cells.

RUNX1 Is Required for Optimal Regulation of FoxP3 Expression

The decreased FoxP3 expression in *Cbfb*-deleted Treg cells suggests that the Runx complex is required for constitutive FoxP3 expression in Treg cells. Because introduction of siRNA against *RUNX1* into human Treg cells efficiently repressed *RUNX1* expression (Ono et al., 2007), we examined the effect of *RUNX1* knockdown on FoxP3 expression in FoxP3-expressing T cell line MT-2 and in primary human $CD4^+CD25^{hi}$ cells. Both MT-2 cells and human Treg cells showed attenuated expression of FoxP3 after *RUNX1* siRNA transfection, indicating a key contribution of RUNX1 to the maintenance of constitutive FoxP3 expression (Figure 6A). Even in the presence of 100 U/ml of IL-2, Treg cells transduced with *RUNX1* siRNA still showed lower FoxP3 expression, indicating that attenuated FoxP3 expression was independent of IL-2 supply (Figure 6B). Further, by RT-PCR, *FOXP3* mRNA expression was slightly but significantly decreased in *Cbfb*-deleted Treg cells and *RUNX1* siRNA-introduced MT-2 cells, indicating that the Runx complex regulated FoxP3 expression, at least in part, at the level of transcription (Figure S6 and Figure 6C). Moreover, with human primary naive $CD4^+$ T cells, in which T cell receptor (TCR) stimulation can induce FoxP3 expression (Mantel et al., 2006; Walker et al., 2003), *RUNX1* knockdown attenuated this activation-induced FoxP3 expression (Figure 6D). This suggests that the Runx complex controls not only constitutive expression of FoxP3 in natural Treg cells but also its de novo induction in activated human $CD4^+$ T cells.

Given that the Runx complex binds to the possible regulatory regions of the *FOXP3* gene, it may directly control *FOXP3* transcription in Treg cells. We thus assessed the direct contribution of the Runx complex to *FOXP3* transcription by reporter gene assays. CNS1 and CNS3 of the human *FOXP3* gene exhibited significant transactivational activities in $CD4^+$ T cells (Figure S11A and Supplemental Data). The mutations of Runx-binding sites in the CNS1 and CNS3 constructs failed to attenuate the transactivational activities observed in those constructs (Figure S11B and Supplemental Data). However, the Runx-site mutations in CNS1 abrogated the transactivation of the construct in response to the stimulation (Figure 6E, left). In contrast to CNS1, the CNS3 construct, either of wild-type or mutant, showed no response to the stimulation (Figure 6E, right). Similar results were also observed in FoxP3-expressing ATL-43T, a human adult T cell leukemia cell line (Figure 6F).

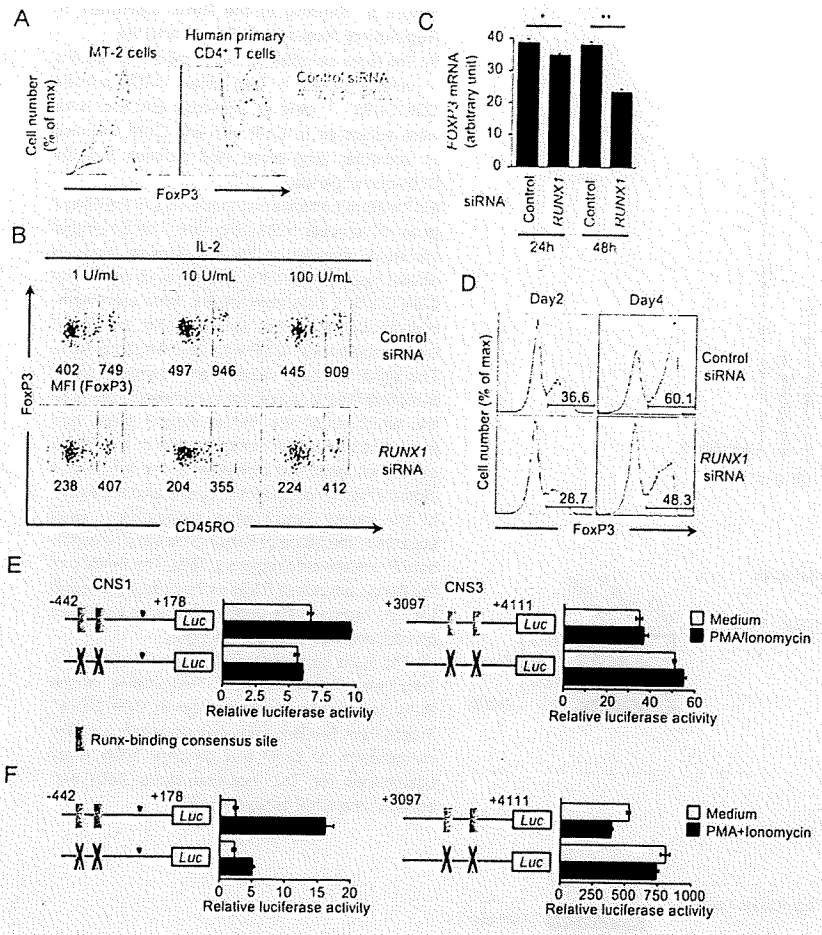

Figure 6. RUNX1 Was Required for Optimal Regulation of FoxP3 Expression

(A) Expression of FoxP3 by MT-2 cells and human primary CD4+ T cells transduced with control or *RUNX1* siRNA 3 days and 4 days after transduction, respectively. Results representative of three experiments are shown.

(B) Effect of exogenous IL-2 on FoxP3 expression by human primary $CD4^+CD25^{hi}CD45RO^-$ naive Treg cells and $CD4^+CD25^{hi}CD45RO^+$ memory Treg cells transduced with control or *RUNX1* siRNA. siRNA-transduced human Treg cells were purified 24 hr after transduction; this process was followed by culture for 3 days in the presence of the indicated concentrations of exogenous IL-2. Numbers shown below the gates indicate the mean fluorescence intensity (MFI) of FoxP3 in the gates. Data are representative of two experiments.

(C) Relative mRNA expression of *FOXP3* in MT-2 cells transduced with control or *RUNX1* siRNA 24 hr and 48 hr after transduction. RNA was extracted from purified PI (propidium iodide)-negative viable MT-2 cells. Results of three experiments are shown as the mean ± SD values. $^*p = 0.01$; $^{**}p = 0.0001$ (unpaired t test).

(D) *RUNX1* knockdown attenuated activation-induced FoxP3 expression in human primary naive $CD4^+$ T cells. siRNA-introduced $CD4^+CD25^-CD45RO^-$ naive T cells were stimulated with anti-CD3 and anti-CD28 in the presence of antigen-presenting cells for 2 or 4 days. Numbers shown above the gates indicate the percentages of $CD4^+FoxP3^+$ cells in $CD4^+$ T cells. Results representative of two experiments are shown.

(E and F) Activation of the *FOXP3* CNS1 by stimulation with PMA and ionomycin is dependent on Runx-binding consensus sequences. The *FOXP3* CNS1 and CNS3 constructs with or without mutations in Runx sites were transfected into human primary $CD4^+$ T cells (E) and ATL 43T cells (F) and cultured in medium or in medium containing PMA and ionomycin. Results shown are the mean ± SD of triplicates done in one experiment representative of three.

Taken together, these results suggest that the Runx complex is required for optimal regulation of FoxP3 expression.

Analyses of *Runx1$^{F/F}$: FIC* and *Runx3$^{F/F}$: FIC* Mice

Because both Runx1 and Runx3 were expressed in Treg cells (Figure S12; Ono et al., 2007), we next investigated which one played a key role for Treg cell function in vivo. We generated *Runx1$^{F/F}$: FIC* and *Runx3$^{F/F}$: FIC* mice by crossing *FIC* mice with *Runx1*-floxed or *Runx3*-floxed mice, respectively (Naoe et al., 2007; Taniuchi et al., 2002). *Runx1$^{F/F}$: FIC* mice developed histologically evident gastritis, high titers of parietal cell antibodies, and hyperproduction of IgE as observed in *Cbfb$^{F/F}$: FIC* mice, whereas IgG production was not significantly altered (Figures 7A–7D). By contrast, *Runx3$^{F/F}$: FIC* mice did not develop gastritis, parietal cell antibodies, or hyperproduction of IgE (Figures 7B–7D). *Runx1*- but not *Runx3*-deleted Treg cells showed attenuated FoxP3 expression as observed in *Cbfb*-deleted Treg cells (Figure 7E). In addition, *Runx1*- or *Runx3*-deleted Treg cells did not lose CD103 expression, whereas *Cbfb*-deleted Treg cells lost it, indicating that Runx1 and Runx3 function redundantly in the regulation of CD103 expression (Figure 7F). Also, the finding indicates that autoimmune phenotypes due to Cbfβ deficiency in Treg cells is not attributed to the loss of CD103 expression because CD103 expression was not altered in autoimmune *Runx1$^{F/F}$: FIC* mice. Our results thus demonstrate that Runx1, but not Runx3, is indispensable for in vivo Treg cell function but do not exclude possible functional compensation between Runx1 and Runx3 in Treg cells.

DISCUSSION

In this study, we showed that Treg cell-specific deficiency of Cbfβ or Runx1, but not Runx3, impaired in vivo Treg cell function, resulting in the development of autoimmune disease and hyperproduction of IgE. The immunological diseases were similar in spectrum to those found in FoxP3 mutant or -deficient mice, although the disease severities were much milder (Sakaguchi et al., 2006).

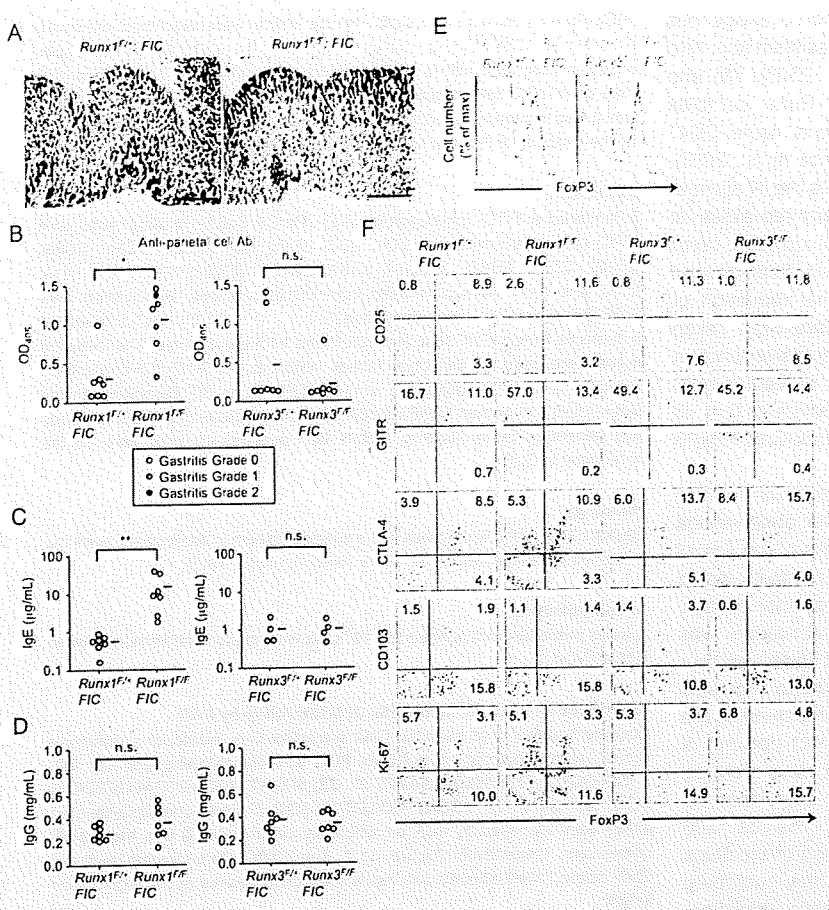

Figure 7. Development of Autoimmune Disease and Hyperproduction of IgE in *Runx1*$^{F/F}$*: FIC* Mice, but Not in *Runx3*$^{F/F}$*: FIC* Mice

(A) Hematoxylin and eosin staining of stomach sections of 8- to 9-week-old *Runx1*$^{F/F}$*: FIC* and *Runx1*$^{F/+}$*: FIC* littermates (n = 7). Representative photomicrographs are shown. Scale bars represent 10.0 μm.

(B) Titers of parietal cell autoantibodies in the sera of 8- to 9-week-old *Runx1*$^{F/F}$*: FIC* and *Runx1*$^{F/+}$*: FIC* littermates (n = 7) (left) and *Runx3*$^{F/F}$*: FIC* and *Runx3*$^{F/+}$*: FIC* littermates (n = 7) (right) were assessed by ELISA. Horizontal lines represent averages from each group. $^{*}p = 0.01$.

(C and D) Titers of IgE (C) and IgG (D) in the sera of 8- to 9-week-old *Runx1*$^{F/F}$*: FIC* and *Runx1*$^{F/+}$*: FIC* littermates (n = 7) and *Runx3*$^{F/F}$*: FIC* and *Runx3*$^{F/+}$*: FIC* littermates (n = 4) were assessed by ELISA. Horizontal lines represent averages from each group. $^{**}p = 0.002$.

(E) Flow cytometric analysis of FoxP3 expression by CD4^{+} T cells from *Runx1*$^{F/F}$*: FIC* and *Runx1*$^{F/+}$*: FIC* littermates (left) and from *Runx3*$^{F/F}$*: FIC* and *Runx3*$^{F/+}$*: FIC* littermates (right) at 7 weeks of age. Results representative of three experiments are shown.

(F) Expression of FoxP3 and the indicated molecules by *Runx1*$^{F/F}$*: FIC* and *Runx1*$^{F/+}$*: FIC* littermates and by *Runx3*$^{F/F}$*: FIC* and *Runx3*$^{F/+}$*: FIC* littermates at 7 to 10 weeks of age. Results representative of three experiments are shown.

We have previously shown that Runx1 binds to the promoter of the *Il2* and *Ifng* genes and enhances IL-2 and IFN-γ production in conventional T cells. Conversely, the FoxP3-Runx1 complex, together with other transcription factors such as NFAT, represses the expression of these cytokines and confers in vitro-suppressive activity to Treg cells (Ono et al., 2007). Here, we have provided genetic evidence that Treg cell-specific deficiency of the Runx1-Cbfβ complex indeed impairs in vivo Treg cell function. This indicates that Runx-dependent gene regulation is critically required for in vivo Treg cell function. In addition, Cbfβ-deficient Treg cells transcribed *Il17a* and *Rorgt* to lesser extents than control Treg cells, whereas *Il4*, *Il10*, and *Tbx21* increased in the former. Other studies have shown that Runx1 induces the expression of RORγt, interacts with RORγt in conventional T cells, and regulates *Il17* transcription via controlling the promoter or enhancer regions of the *Il17* gene (Zhang et al., 2008). Runx3 also acts with T-bet to activate *Ifng* and silence *Il4* via binding to the *Ifng* promoter and the *Il4* silencer regions, respectively, leading to Th1 cell-specific cytokine production (Djuretic et al., 2007). Further, Runx1 and Runx3 interact with the *Cd4* silencer and the *Zbtb7b* silencer, in regulating thymocyte commitment to the CD8^{+} T cell lineage by repressing the alternative cell fate (Setoguchi et al., 2008; Taniuchi et al., 2002). Thus, the Runx complex plays critical roles not only in T cell differentiation, in particular CD4-CD8 lineage commitment, but also in conferring a variety of functions to T cell subsets including Th1, Th17, and Treg cell. Further, phenotypical differences between *Runx1*- and *Runx3*-deleted Treg cells suggest that Runx1 and Runx3 differently contribute to the differentiation and the functions of T cell subsets. The Runx complex may thus function as an essential core transcriptional "modifier" to regulate specialized effector functions of CD4^{+} T cell subsets by associating with particular lineage-specific transcription factors including FoxP3.

Regarding the mechanism by which Treg cell function is impaired in Cbfβ- or Runx1-deficient Treg cells, a notable finding is that Cbfβ or Runx1 deficiency accompanies attenuated expression of FoxP3 at mRNA and protein levels. Because attenuated FoxP3 expression can lead to loss of Treg cell-suppressive function, as demonstrated by others (Wan and Flavell, 2007), reduced expression of FoxP3 might be responsible for dysfunction of *Cbfb*-deleted Treg cells. For example, *Nrp1* and *Pde3b*, which were differentially expressed in *Cbfb*-deleted Treg cells by expression microarray, could be affected by FoxP3 hypoexpression. Other differentially expressed genes are also possibly associated with the impaired function of *Cbfb*-deleted Treg cells. They include *Il4*, *Ltb4r1*, *Cd160*, and *Ccr5*, all of which were overexpressed in *Cbfb*-deleted Treg cells. Of particular note is the hyperproduction of IL-4 by *Cbfb*-deleted Treg cells. Elevated IL-4 may contribute to the impaired Treg cell-mediated suppression in *Cbfb*- or *Runx1*-deleted Treg

cells because it has been shown that the addition of exogenous IL-4 renders $CD4^+CD25^-$ conventional T cells resistant to in vitro Treg cell-mediated suppression (Pace et al., 2006). We and others have previously reported that the Runx complex represses *Il4* via binding to the *Il4* silencer in naive $CD4^+$ T cells and Th1 cells (Djuretic et al., 2007; Naoe et al., 2007). Our observation that the Runx complex bound to the *Il4* silencer in Treg cells suggests that the complex similarly represses *Il4* expression in Treg cells and that loss of Runx complex derepresses *Il4*, leading to hyperproduction of IL-4 in *Cbfb*-deleted Treg cells. Nonetheless, it is also possible that reduction of FoxP3 expression directly derepresses *Il4* expression. Taken together, our findings show that impaired suppressive function of *Cbfb*-deleted Treg cells could be attributed, at least in part, to the reduction of FoxP3 and the hyperproduction of IL-4, in addition to the impaired formation of the Runx-Cbfβ-FoxP3 complex (Ono et al., 2007).

The maintenance of constitutive FoxP3 expression in Treg cells appears to require the Runx complex. Our observations that the complex bound to the regulatory regions of the *Foxp3* gene in Treg cells may suggest that the Runx complex would directly upregulate FoxP3 expression. In the reporter assays, however, Runx-binding site-dependent transactivation was observed only under activated condition, and not under unstimulated condition. This suggests that the Runx complex regulates constitutive FoxP3 expression more than by transactivating the *FOXP3* gene. It has also been shown that RUNX1 not only is a conventional transcriptional activator but also plays a critical role in chromatin modifications such as histone acetylation via interacting with histone acetyltransferases (Yoshida and Kitabayashi, 2008). This suggests that the binding of the Runx complex to the *Foxp3* gene regulatory regions may contribute to constitutive FoxP3 expression through epigenetic regulation. It is also possible that the deficiency of the Runx complex may primarily dysregulate other genes encoding molecules necessary for the maintenance of FoxP3 expression in Treg cells. These possibilities are currently under investigation.

Our results support the concept that Runx-dependent program plays essential roles for immune homeostasis including Treg cell-mediated immune suppression. Single-nucleotide polymorphisms (SNPs) affecting the consensus sites for RUNX1 are associated with the genetic susceptibility to several autoimmune diseases including systemic lupus erythematosus, rheumatoid arthritis, and psoriasis (Alarcon-Riquelme, 2004; Helms et al., 2003; Prokunina et al., 2002; Tokuhiro et al., 2003). In addition, a SNP in the *RUNX1* gene itself was strongly associated with rheumatoid arthritis (Tokuhiro et al., 2003). It is thus likely that genetic alterations of *RUNX1* may contribute to the development of autoimmune diseases in part by means of affecting Treg cell-mediated immune regulation. Furthermore, our study suggests that Treg cell-specific inhibition of the activity of the Runx1-Cbfβ complex could be useful for reducing Treg cell activity and thereby evoking effective tumor immunity.

EXPERIMENTAL PROCEDURES

Mice

C.B-17 SCID mice were purchased from CLEA Japan (Tokyo, Japan). BALB/c mice were purchased from Japan SLC (Shizuoka, Japan). *Foxp3-Ires-Cre (FIC)*, *Runx1*^{F}, *Runx3*^{F}, and *Cbfb*^{F} mouse strains were described previously (Naoe et al., 2007; Taniuchi et al., 2002; Wang et al., 2008). In this paper, a mouse described with a "*FIC*" genotype was either a *FIC/Y* hemizygote male or *FIC/FIC* homozygote female. All mice were maintained in our animal facility and treated in accordance with the guidelines for animal care approved by the Institute for Frontier Medical Sciences, Kyoto University.

Antibodies

Biotinylated or FITC-, phycoerythrin (PE)-, PerCP-Cy5.5-, or allophycocyanin (APC)-conjugated mAbs for CD4, CD8, CD25, HSA (CD24), TCRβ, CD69, CD122, CD44, CD62L, CTLA-4, Ki-67, CD127, CD103, IFN-γ, IL-2, IL-4, IL-10, and IL-17 were purchased from BD Biosciences. Biotinylated anti-GITR (DTA1) was previously described (Shimizu et al., 2002). APC-conjugated anti-mouse Foxp3 (FJK-16 s) was purchased from eBioscience. The following mAbs were used for detecting human antigens: PerCP-Cy5.5-conjugated anti-CD4 and FITC-conjugated anti-CD45RO from BD Biosciences and biotinylated anti-human FOXP3 (236A/E7) from eBiosciences. Cbfβ antibody was generated by immunizing rabbits with peptides corresponding to the N-terminal of Cbfβ.

Histology

Gastritis and colitis were graded in a blinded fashion in accordance with the published criteria (Asano et al., 1996; Asseman et al., 1999).

Immunoblotting

Lysates prepared from purified 5×10^3 cells were loaded and immunoblotted with anti-Cbfβ.

Identification of *Cbfb*^{F} and *Cbfb*-Deleted Allele by PCR

Equivalent amounts of genomic DNA extracted from individual lymphocyte subset were subjected to multiplex PCR with the following primers: G2, 5′-CCTCCTCATTCTAACAGGAATC-3′; G3, 5′-GGTTAGGAGTCATTGTGATC AC-3′; and G6, 5′-CATTGGATTGGCGTTACTGG-3′. *Cbfb*^{F} and *Cbfb*-deleted alleles were identified by PCR amplification with the G3/G2 and the G3/G6 primer pair, respectively (Figure S13). The *Cbfb*^{F} allele-specific and the *Cbfb*-deleted allele-specific amplicons were distinguished according to their length.

ELISA

Autoantibodies specific for gastric parietal cells were detected by ELISA as previously described (Sakaguchi et al., 1995). Serum IgG and IgE levels were assessed by ELISA with Mouse IgG ELISA Quantitation Kit (Bethyl Laboratories) and OptEIA Mouse IgE ELISA set (BD Biosciences), respectively.

Cell Sorting

Fresh mouse $CD4^+$ T cells were isolated as previously described (Hori et al., 2003). Then, $CD4^+$ T cell subpopulations including $CD4^+CD25^{hi}$ cells, $CD4^+CD25^-$ cells, and $CD4^+CD25^-CD45RB^{hi}$ cells were purified by sorting with a cell sorter (MoFlo, Dako). In some experiments, $CD4^+CD25^+$ cells were purified by MACS (Miltenyi Biotec).

Intracellular Cytokine Staining

Cells were stimulated for 5 hr with 20 ng/ml phorbol 12-myristate 13-acetate (PMA) and 1 μM ionomycin in the presence of GolgiStop (BD Biosciences). For intracellular cytokine staining, stimulated cells were stained for surface antigens, fixed, permeabilized with BD Cytofix/Cytoperm (BD Biosciences), and stained by anti-cytokine. For costaining of intracellular cytokine and FoxP3, stimulated cells were stained for surface antigens, fixed, permeabilized with Foxp3 Fixation/Permeabilization Kit (eBioscience), and finally, costained with cytokine antibody and Foxp3 antibody.

Proliferation Assay and Suppression Assay

A total of 2×10^4 responder T cells were cultured with or without graded numbers of suppressor cells for 3 days in the presence of 4×10^4 antigen-presenting cells (mitomycin C-treated $Thy1.2^+$ cell-depleted BALB/c splenocytes) and 0.5 μg/ml CD3 antibody (145-2C11, BD Biosciences). [^{3}H]thymidine (1 μCi/well) was added during the last 8 hr of culture.

Quantitative Real-Time RT-PCR

Total RNA was prepared from cells of interest with RNeasy Mini Kit (QIAGEN). cDNA was synthesized from total RNA with SuperScript III reverse transcriptase and oligo(dT)$_{12-18}$ primer (Invitrogen). Quantitative real-time RT-PCR was performed with the LightCycler 480 System (Roche Applied Science) with QuantiTect SYBR Green PCR Kit (QIAGEN). Primer pairs used are listed in Table S4. All samples were run in triplicate and the data were normalized to *Hprt* mRNA expression.

Chromatin Immunoprecipitation and Tiling Array

Cells were crosslinked by the addition of one-tenth volume of fresh 11% formaldehyde solution for 10 min at room temperature. Cells were resuspended, lysed in lysis buffers, and sonicated for solubilization and shearing of crosslinked DNA. The cell extract was incubated overnight at 4 C with 100 μl of Dynal anti-rabbit IgG magnetic beads that had been preincubated with 10 μg of the Cbfβ antibody. Beads were washed five times with RIPA buffer and one time with TE containing 50 mM NaCl. Bound complexes were eluted from the beads by heating at 65 C with occasional vortexing, and crosslinking was reversed by overnight incubation at 65 C. Immunoprecipitated DNA and whole-cell extract DNA were then purified by treatment with RNaseA, proteinase K, and multiple phenol:chloroform:isoamyl alcohol extractions. For conventional ChIP assays, the precipitated DNA was subjected to PCR amplification. The primers used are as follows: FxCNS1-for, 5′-AGCCCTGT TATCTCATTGATAC-3′; FxCNS1-rev, 5′-GACCTCGCTCTTCTAATAATCC-3′; FxCNS2-for, 5′-CCCATACCCACACTTTTGACCTCTG-3′; FxCNS2-rev, 5′-GC ACTTGAAAATGAGATAACTGTTCA-3′; FxCNS3-for, 5′-CTGGCATCCAAGAA AGACA-3′; and FxCNS3-rev, 5′-GGCTTCATCGGCAACAA-3′. Primers for *Il4* silencer region and for the region at 1 kb upstream of *Zbtb7b* (*Th-POK*) exon Ia (UP1) were described previously (Naoe et al., 2007; Setoguchi et al., 2008). For a ChIP-on-chip experiment, purified DNA was amplified twice by LM-PCR in accordance with the manufacturer's protocol (Agilent). We used mouse promoter array and custom microarrays generated by Agilent that tiled through several loci via 60-nucleotide oligonucleotide probes. The probes, representing the forward strand, were spaced every 200 bases and were printed at random location on the array. Probe hybridization and scanning of oligonucleotide array data were performed in accordance with the manufacturer's protocol (Agilent). Data analyses were carried out with Feature Extraction software and ChIP Analytics software (Agilent).

RNA Interference

MT-2 cells and MACS-sorted primary human CD4$^+$ T cells were transduced with *RUNX1* siRNA (HSS141472; Invitrogen) or Stealth RNAi negative control GC high (Invitrogen) as previously described (Ono et al., 2007).

Expression Microarray

Total RNA was isolated with the RNeasy Micro Kit (QIAGEN). Biotinylated antisense cRNA was prepared by two cycles of in vitro amplication. Biotinylated cRNA (15 μg) was hybridized to Affymetrix GeneChip Mouse Genome 430 2.0 arrays. Data analyses were done with the use of MeV (v4.2) (Saeed et al., 2003).

Induction of FoxP3 Expression in Human Naive T Cells

CD25$^-$CD45RO$^-$ primary human naive T cells were negatively sorted with MACS Pan T Cell Isolation Kit II, CD25 MicroBeads, and CD45RO MicroBeads (Miltenyi Biotec). A total of 7 × 10^6 purified naive T cells were transduced with control or *RUNX1* siRNA with a Human T Cell Nucleofector Kit (Amaxa), mixed with 4 × 10^6 T cell-depleted syngeneic PBMCs, and then cultured in a volume of 1 ml (12-well plates) for 24 h. Then, 7 × 10^5 cells were harvested and cultured in a volume of 200 μl (96-well plates) in the presence of 0.01 μg/ml anti-CD3 (OKT3) and 0.02 μg/ml anti-CD28 (CD28.2) for 4 days. Blood samples were obtained from healthy adult volunteers (20–40 years old). The study was conducted with the approval from the human ethics committee of the Institute for Frontier Medical Sciences, Kyoto University.

Statistical analysis

Comparisons were analyzed for statistical significance by Mann-Whitney U test, unless otherwise stated, with $p < 0.05$ being considered significant.

ACCESSION NUMBERS

Microarray data are available from the National Center for Biotechnology Information Gene Expression Omnibus (GEO) under accession number GSE18148.

SUPPLEMENTAL DATA

Supplemental Data include 13 figures, 5 tables, and Supplemental Experimental Procedures and can be found with this article online at http://www.cell.com/immunity/supplemental/S1074-7613(09)00407-5.

ACKNOWLEDGMENTS

We thank M. Kakino, R. Ishii, M. Yoshida, and K. Akiyama for technical assistance; M. Matsuoka for ATL-43T cell line; and M. Matsushita for preparing histology.

Received: August 24, 2009
Revised: September 9, 2009
Accepted: September 14, 2009
Published online: October 1, 2009

REFERENCES

Alarcon-Riquelme, M.E. (2004). Role of RUNX in autoimmune diseases linking rheumatoid arthritis, psoriasis and lupus. Arthritis Res. Ther. *6*, 169–173.

Annacker, O., Coombes, J.L., Malmstrom, V., Uhlig, H.H., Bourne, T., Johansson-Lindbom, B., Agace, W.W., Parker, C.M., and Powrie, F. (2005). Essential role for CD103 in the T cell-mediated regulation of experimental colitis. J. Exp. Med. *202*, 1051–1061.

Asano, M., Toda, M., Sakaguchi, N., and Sakaguchi, S. (1996). Autoimmune disease as a consequence of developmental abnormality of a T cell subpopulation. J. Exp. Med. *184*, 387–396.

Asseman, C., Mauze, S., Leach, M.W., Coffman, R.L., and Powrie, F. (1999). An essential role for interleukin 10 in the function of regulatory T cells that inhibit intestinal inflammation. J. Exp. Med. *190*, 995–1004.

Bettelli, E., Dastrange, M., and Oukka, M. (2005). Foxp3 interacts with nuclear factor of activated T cells and NF-kappa B to repress cytokine gene expression and effector functions of T helper cells. Proc. Natl. Acad. Sci. USA *102*, 5138–5143.

Cao, X., Cai, S.F., Fehniger, T.A., Song, J., Collins, L.I., Piwnica-Worms, D.R., and Ley, T.J. (2007). Granzyme B and perforin are important for regulatory T cell-mediated suppression of tumor clearance. Immunity *27*, 635–646.

de Bruijn, M.F., and Speck, N.A. (2004). Core-binding factors in hematopoiesis and immune function. Oncogene *23*, 4238–4248.

Djuretic, I.M., Levanon, D., Negreanu, V., Groner, Y., Rao, A., and Ansel, K.M. (2007). Transcription factors T-bet and Runx3 cooperate to activate Ifng and silence Il4 in T helper type 1 cells. Nat. Immunol. *8*, 145–153.

Durst, K.L., and Hiebert, S.W. (2004). Role of RUNX family members in transcriptional repression and gene silencing. Oncogene *23*, 4220–4224.

Egawa, T., Tillman, R.E., Naoe, Y., Taniuchi, I., and Littman, D.R. (2007). The role of the Runx transcription factors in thymocyte differentiation and in homeostasis of naive T cells. J. Exp. Med. *204*, 1945–1957.

Fontenot, J.D., Gavin, M.A., and Rudensky, A.Y. (2003). Foxp3 programs the development and function of CD4+CD25+ regulatory T cells. Nat. Immunol. *4*, 330–336.

Gondek, D.C., Lu, L.F., Quezada, S.A., Sakaguchi, S., and Noelle, R.J. (2005). Cutting edge: Contact-mediated suppression by CD4+CD25+ regulatory cells involves a granzyme B-dependent, perforin-independent mechanism. J. Immunol. *174*, 1783–1786.

Grueter, B., Petter, M., Egawa, T., Laule-Kilian, K., Aldrian, C.J., Wuerch, A., Ludwig, Y., Fukuyama, H., Wardemann, H., Waldschuetz, R., et al. (2005). Runx3 regulates integrin alpha E/CD103 and CD4 expression during development of CD4-/CD8+ T cells. J. Immunol. *175*, 1694–1705.

Helms, C., Cao, L., Krueger, J.G., Wijsman, E.M., Chamian, F., Gordon, D., Heffernan, M., Daw, J.A., Robarge, J., Ott, J., et al. (2003). A putative RUNX1 binding site variant between SLC9A3R1 and NAT9 is associated with susceptibility to psoriasis. Nat. Genet. *35*, 349–356.

Hill, J.A., Feuerer, M., Tash, K., Haxhinasto, S., Perez, J., Melamed, R., Mathis, D., and Benoist, C. (2007). Foxp3 transcription-factor-dependent and -independent regulation of the regulatory T cell transcriptional signature. Immunity *27*, 786–800.

Hori, S., Nomura, T., and Sakaguchi, S. (2003). Control of regulatory T cell development by the transcription factor Foxp3. Science *299*, 1057–1061.

Khattri, R., Cox, T., Yasayko, S.A., and Ramsdell, F. (2003). An essential role for Scurfin in CD4+CD25+ T regulatory cells. Nat. Immunol. *4*, 337–342.

Kim, H.P., and Leonard, W.J. (2007). CREB/ATF-dependent T cell receptor-induced FoxP3 gene expression: A role for DNA methylation. J. Exp. Med. *204*, 1543–1551.

Komine, O., Hayashi, K., Natsume, W., Watanabe, T., Seki, Y., Seki, N., Yagi, R., Sukzuki, W., Tamauchi, H., Hozumi, K., et al. (2003). The Runx1 transcription factor inhibits the differentiation of naive CD4+ T cells into the Th2 lineage by repressing GATA3 expression. J. Exp. Med. *198*, 51–61.

Li, B., Samanta, A., Song, X., Iacono, K.T., Bembas, K., Tao, R., Basu, S., Riley, J.L., Hancock, W.W., Shen, Y., et al. (2007). FOXP3 interactions with histone acetyltransferase and class II histone deacetylases are required for repression. Proc. Natl. Acad. Sci. USA *104*, 4571–4576.

Mantel, P.Y., Ouaked, N., Ruckert, B., Karagiannidis, C., Welz, R., Blaser, K., and Schmidt-Weber, C.B. (2006). Molecular mechanisms underlying FOXP3 induction in human T cells. J. Immunol. *176*, 3593–3602.

Naoe, Y., Setoguchi, R., Akiyama, K., Muroi, S., Kuroda, M., Hatam, F., Littman, D.R., and Taniuchi, I. (2007). Repression of interleukin-4 in T helper type 1 cells by Runx/Cbf beta binding to the Il4 silencer. J. Exp. Med. *204*, 1749–1755.

Ochs, H.D., Ziegler, S.F., and Torgerson, T.R. (2005). FOXP3 acts as a rheostat of the immune response. Immunol. Rev. *203*, 156–164.

Ono, M., Yaguchi, H., Ohkura, N., Kitabayashi, I., Nagamura, Y., Nomura, T., Miyachi, Y., Tsukada, T., and Sakaguchi, S. (2007). Foxp3 controls regulatory T-cell function by interacting with AML1/Runx1. Nature *446*, 685–689.

Pace, L., Rizzo, S., Palombi, C., Brombacher, F., and Doria, G. (2006). Cutting edge: IL-4-induced protection of CD4+CD25- Th cells from CD4+CD25+ regulatory T cell-mediated suppression. J. Immunol. *176*, 3900–3904.

Prokunina, L., Castillejo-Lopez, C., Oberg, F., Gunnarsson, I., Berg, L., Magnusson, V., Brookes, A.J., Tentler, D., Kristjansdottir, H., Grondal, G., et al. (2002). A regulatory polymorphism in PDCD1 is associated with susceptibility to systemic lupus erythematosus in humans. Nat. Genet. *32*, 666–669.

Saeed, A.I., Sharov, V., White, J., Li, J., Liang, W., Bhagabati, N., Braisted, J., Klapa, M., Currier, T., Thiagarajan, M., et al. (2003). TM4: A free, open-source system for microarray data management and analysis. Biotechniques *34*, 374–378.

Sakaguchi, S., Ono, M., Setoguchi, R., Yagi, H., Hori, S., Fehervari, Z., Shimizu, J., Takahashi, T., and Nomura, T. (2006). Foxp3+ CD25+ CD4+ natural regulatory T cells in dominant self-tolerance and autoimmune disease. Immunol. Rev. *212*, 8–27.

Sakaguchi, S., Sakaguchi, N., Asano, M., Itoh, M., and Toda, M. (1995). Immunologic self-tolerance maintained by activated T cells expressing IL-2 receptor alpha-chains (CD25). Breakdown of a single mechanism of self-tolerance causes various autoimmune diseases. J. Immunol. *155*, 1151–1164.

Sato, T., Ohno, S., Hayashi, T., Sato, C., Kohu, K., Satake, M., and Habu, S. (2005). Dual functions of Runx proteins for reactivating CD8 and silencing CD4 at the commitment process into CD8 thymocytes. Immunity *22*, 317–328.

Setoguchi, R., Tachibana, M., Naoe, Y., Muroi, S., Akiyama, K., Tezuka, C., Okuda, T., and Taniuchi, I. (2008). Repression of the transcription factor Th-POK by Runx complexes in cytotoxic T cell development. Science *319*, 822–825.

Shimizu, J., Yamazaki, S., Takahashi, T., Ishida, Y., and Sakaguchi, S. (2002). Stimulation of CD25(+)CD4(+) regulatory T cells through GITR breaks immunological self-tolerance. Nat. Immunol. *3*, 135–142.

Speck, N.A. (2001). Core binding factor and its role in normal hematopoietic development. Curr. Opin. Hematol. *8*, 192–196.

Taniuchi, I., and Littman, D.R. (2004). Epigenetic gene silencing by Runx proteins. Oncogene *23*, 4341–4345.

Taniuchi, I., Osato, M., Egawa, T., Sunshine, M.J., Bae, S.C., Komori, T., Ito, Y., and Littman, D.R. (2002). Differential requirements for Runx proteins in CD4 repression and epigenetic silencing during T lymphocyte development. Cell *111*, 621–633.

Tokuhiro, S., Yamada, R., Chang, X., Suzuki, A., Kochi, Y., Sawada, T., Suzuki, M., Nagasaki, M., Ohtsuki, M., Ono, M., et al. (2003). An intronic SNP in a RUNX1 binding site of SLC22A4, encoding an organic cation transporter, is associated with rheumatoid arthritis. Nat. Genet. *35*, 341–348.

Tone, Y., Furuuchi, K., Kojima, Y., Tykocinski, M.L., Greene, M.I., and Tone, M. (2008). Smad3 and NFAT cooperate to induce Foxp3 expression through its enhancer. Nat. Immunol. *9*, 194–202.

van Wijnen, A.J., Stein, G.S., Gergen, J.P., Groner, Y., Hiebert, S.W., Ito, Y., Liu, P., Neil, J.C., Ohki, M., and Speck, N. (2004). Nomenclature for Runt-related (RUNX) proteins. Oncogene *23*, 4209–4210.

Walker, M.R., Kasprowicz, D.J., Gersuk, V.H., Benard, A., Van Landeghen, M., Buckner, J.H., and Ziegler, S.F. (2003). Induction of FoxP3 and acquisition of T regulatory activity by stimulated human CD4+CD25- T cells. J. Clin. Invest. *112*, 1437–1443.

Wan, Y.Y., and Flavell, R.A. (2007). Regulatory T-cell functions are subverted and converted owing to attenuated Foxp3 expression. Nature *445*, 766–770.

Wing, K., Onishi, Y., Prieto-Martin, P., Yamaguchi, T., Miyara, M., Fehervari, Z., Nomura, T., and Sakaguchi, S. (2008). CTLA-4 control over Foxp3+ regulatory T cell function. Science *322*, 271–275.

Woolf, E., Xiao, C., Fainaru, O., Lotem, J., Rosen, D., Negreanu, V., Bernstein, Y., Goldenberg, D., Brenner, O., Berke, G., et al. (2003). Runx3 and Runx1 are required for CD8 T cell development during thymopoiesis. Proc. Natl. Acad. Sci. USA *100*, 7731–7736.

Wu, Y., Borde, M., Heissmeyer, V., Feuerer, M., Lapan, A.D., Stroud, J.C., Bates, D.L., Guo, L., Han, A., Ziegler, S.F., et al. (2006). FOXP3 controls regulatory T cell function through cooperation with NFAT. Cell *126*, 375–387.

Yoshida, H., and Kitabayashi, I. (2008). Chromatin regulation by AML1 complex. Int. J. Hematol. *87*, 19–24.

Zhang, F., Meng, G., and Strober, W. (2008). Interactions among the transcription factors Runx1, RORgammat and Foxp3 regulate the differentiation of interleukin 17-producing T cells. Nat. Immunol. *9*, 1297–1306.

Developmental Biology 329 (2009) 176–190

Contents lists available at ScienceDirect

Developmental Biology

journal homepage: www.elsevier.com/developmentalbiology

Brpf1, a subunit of the MOZ histone acetyl transferase complex, maintains expression of anterior and posterior *Hox* genes for proper patterning of craniofacial and caudal skeletons

Kenta Hibiya [a], Takuo Katsumoto [b], Takashi Kondo [c], Issay Kitabayashi [b], Akira Kudo [a,*]

[a] Department of Biological Information, Tokyo Institute of Technology, 4259-B-23 Midori-ku, Nagatsuta, Yokohama 226-8501, Japan
[b] Molecular Oncology Division, National Cancer Center Research Institute, 5-1-1 Tukiji, Chuo-ku, Tokyo, 104-0045, Japan
[c] Kondo Research Unit, Neuro-Developmental Disorder Research Group, Brain Science Institute, Institute of Physical and Chemical Research (RIKEN), 2-1 Hirosawa, Wako, Saitama 351-0198, Japan

ARTICLE INFO

Article history:
Received for publication 10 October 2008
Revised 22 January 2009
Accepted 18 February 2009
Available online 27 February 2009

Keywords:
Brpf1
Moz
TrxG
Medaka
Mutant
bis
Hox
Skeleton
Fin ray

ABSTRACT

The epigenetic mechanism involving chromatin modification plays a critical role in the maintenance of the expression of *Hox* genes. Here, we characterize a mutant of the medaka fish, named *biaxial symmetries* (*bis*), in which *brpf1*, a subunit of the MOZ histone acetyl transferase (HAT) complex, is mutated. The *bis* mutant displayed patterning defects both in the anterior–posterior axis of the craniofacial skeleton and the dorsal–ventral axis of the caudal one. In the anterior region, the *bis* mutant exhibited craniofacial cartilage homeosis. The expression of *Hox* genes was decreased in the pharyngeal arches, suggesting that the pharyngeal segmental identities were altered in the *bis* mutant. In the posterior region, the *bis* mutant exhibited abnormal patterning of the caudal skeleton, which ectopically formed at the dorsal side of the caudal fin. The expression of *Zic* genes was decreased at the posterior region, suggesting that the dorsal–ventral axis formation of the posterior trunk was disrupted in the *bis* mutant. We also found that the MOZ-deficient mice exhibited an abnormal patterning of their craniofacial and cervical skeletons and a decrease of Hox transcripts. We propose a common role of the MOZ HAT complex in vertebrates, a complex which is required for the proper patterning for skeletal development.

Introduction

Determination of 3 axes, i.e., the anterior–posterior (A–P) axis, dorsal–ventral (D–V) axis, and left–right (L–R) axis, underlies the developmental processes of a vertebrate embryo as it forms from the fertilized egg to achieve the proper morphology (Beddington and Robertson, 1999; Kuratani, 2005). The A–P axis is governed by *Hox* genes, which encode homeodomain-containing transcription factors. *Hox* genes were first described in *Drosophila* for their ability to cause segmental homeotic transformation in the body plan (Lewis, 1978; Wellik, 2007). A co-linear relationship exists between the relative orders of *Hox* genes. Genes at the 3′ end of the Hox clusters are activated first in the most-anterior parts of the developing embryo, whereas genes located at the more 5′ genomic position of the Hox clusters are activated subsequently in the more posterior parts (Frohman et al., 1993; Kmita and Duboule, 2003; Kondo and Duboule, 1999). The existence of a 'Hox code' has been proposed to assign morphologies to each segment as a result of the combination of the expression of each *Hox* gene (Kuratani, 2005; Wellik, 2007).

Anteriorly, the craniofacial skeleton is derived from the head segmented pharyngeal arch, the fate of which is determined by *Hox* genes located at the 3′ end of the chromosome (Piotrowski and Nusslein-Volhard, 2000). For instance, targeted inactivation of Hoxa2 in mice causes homeotic transformation of the second arch to the skeletal element derived from the first arch with reverse polarity (Gendron-Maguire et al., 1993; Rancourt et al., 1995; Santagati et al., 2005). Posteriorly, the fate of the skeletal identity in the tail region is determined by *Hox* genes located at the 5′ end of the chromosome (Wellik and Capecchi, 2003). Targeted disruption of Hox13 groups results in an anterior shift of morphology of the vertebrae (Dolle et al., 1993; Economides et al., 2003; Godwin and Capecchi, 1998). Thus, the proper regulation of *Hox* genes is required for the proper morphology along the A–P axis.

The expression of *Hox* genes is regulated in dual phases: an early phase, in which the initial expression pattern of *Hox* genes is established along the A–P axis, and a late phase, in which the expression pattern is sustained during further development (Deschamps et al., 1999; Deschamps and van Nes, 2005). The initiation of the expression of *Hox* genes depends on fibroblast growth factor (Fgf) and retinoic acid (RA) signals, and the counter gradients of Fgf and RA signals control the A–P axis formation via regulation of the expression of these *Hox* genes (Bel-Vialar et al., 2002; Deschamps and

* Corresponding author. Fax: +81 45 924 5718.
E-mail address: akudo@bio.titech.ac.jp (A. Kudo).

0012-1606/$ – see front matter © 2009 Elsevier Inc. All rights reserved.
doi:10.1016/j.ydbio.2009.02.021

van Nes, 2005; Diez del Corral and Storey, 2004). Maintenance of stable expression patterns of the *Hox* genes is regulated by the *Polycomb*-group (PcG) and *Trithorax* group (TrxG) of proteins, which are involved in the epigenetic mechanism via modulating the chromatin structure. Previous reports have demonstrated that PcG proteins repress the expression of *Hox* genes, whereas TrxG proteins maintain the active state of their expression (Papp and Muller, 2006; Soshnikova and Duboule, 2008). In mammals, targeted disruption of PcG genes; *bmi*, *mel-18*, *m33*, and *rae28*, causes an anterior shift of the expression of *Hox* genes, which results in the homeotic transformation of vertebrae to posterior segmental identities (Akasaka et al., 1996; Akasaka et al., 2001; Core et al., 1997; del Mar Lorente et al., 2000; Suzuki et al., 2002; Takihara et al., 1997). Targeted disruption of a mammalian *trx* gene, *mll* in mice, causes a gradual reduction in the expression of *Hox* genes during development (Glaser et al., 2006; Yu et al., 1998, 1995). In addition, a histone acetyltransferase (HAT) of the MYST family, Moz (Myst3), which has been implicated to act as a TrxG, is required for the maintenance of the expression of *Hox* genes in the pharyngeal arches during zebrafish embryogenesis (Miller et al., 2004). Although these studies on PcG and TrxG genes have shown several alterations of *Hox* gene expression in restricted regions of developing embryos, PcG and TrxG functions in the transcriptional regulation of *Hox* genes, especially TrxG functions, have not been adequately demonstrated.

In this study, we isolated and characterized a mutant in medaka named *biaxial symmetries* (*bis*), a mutant which displays patterning defects not only in the A–P axis of its craniofacial skeleton but also in the D–V axis of its caudal fin. In the *bis* mutant, the craniofacial skeleton was homeotically transformed into one with anterior morphology. The expression of *Hox* genes was decreased in the pharyngeal arches in the *bis* mutant, suggesting that the segmental identities of pharyngeal arches had been disrupted. Positional cloning revealed a loss of Brpf1 function in the *bis* mutant. Brpf1, containing a bromodomain and PHD finger, is a TrxG member and a close partner of the MOZ HAT complex (Doyon et al., 2006; Rokudai et al., 2009). This study revealed that Brpf1 is essential for the maintenance of expression of *Hox* genes not only in the anterior region, but also in the posterior region. In the posterior trunk, disruption of Brpf1 function caused decreased expression of *Zic* genes, which regulate the D–V axis of the caudal fin. Furthermore, we characterized the skeletal abnormality of the MOZ-deficient mice, and demonstrated similar abnormalities between the *brpf1* medaka mutant and MOZ-deficient mice, thus implying a common role of the MOZ HAT complex in the skeletal patterning of vertebrates.

Methods

Medaka strains and mutant screening

The medaka (*Oryzias latipes*) strain Cab was used for all studies as the wild type. The *Da* mutant was purchased from local pet shops. The fish were maintained in an aquarium system with re-circulating water at 28.5 °C. Naturally spawned embryos were obtained, incubated at 28 °C, and staged as previously described (Iwamatsu, 2004). Eggs were maintained in the medaka Ringer's solution (0.65% NaCl, 0.04% KCl, 0.011% CaCl2, 0.01% $MgSO_4$, 0.01% $NaHCO_3$, 0.0001% methylene blue).

Mutagenesis using N-ethyl-N-nitrosourea (ENU) was performed according to a standard protocol established for zebrafish (Mullins et al., 1994; Solnica-Krezel et al., 1994; van Eeden et al., 1999), with some modifications (Tanaka et al., 2004). The male fish were exposed to 2.5 or 3 mM ENU for 2 h at room temperature in a buffer containing 0.03% instant ocean (Tetra) and 1 mM sodium phosphate buffer at pH 6.5. The ENU treatment was repeated at 7 days after the initial treatment. Three weeks after the second ENU treatment, these male fish were crossed with the wild-type females to produce families of F1 fish. The F1 fish were then mated to each other to obtain F2 families. For each F2 family, random crosses (up to 8 pairs) were made to obtain the F3 progeny. Embryos and larvae were observed for their mutant phenotypes under a stereomicroscope at 3 different stages (3, 5–6, and 9–10 days after fertilization).

Whole-mount RNA in situ hybridization and skeletal staining

Whole-mount RNA *in situ* hybridization using digoxigenin-labeled anti-sense RNA probes was performed as previously described (Inohaya et al., 1995, 1999). For cartilage staining with Alcian blue 8GX (Sigma), larvae were fixed with 4% paraformaldehyde (Sigma) in PBS at 4 °C overnight, washed twice in PBS containing 0.1% Tween (PBST) for 10 min, and stained with the Alcian blue solution (70% ethanol, 30% acetic acid containing 0.1% Alcian blue) at room temperature overnight. Larvae were hydrated by passage through a graded series of PBS and decolorized in a solution of 1% KOH and 0.9% hydrogen peroxide. Then the larvae were treated at room temperature for less than 1 h with 0.1% trypsin (DIFCO) in a 30% sodium borate saturated solution. The calcified bone was stained with Alizarin red S (Nacalai Tesque). For this staining, larvae were fixed in 4% paraformaldehyde with 0.05 N sodium hydroxide at 4 °C overnight. After a brief washing in PBST, the fixed larvae were stained by immersion in the Alizarin red solution (4% Alizarin red, 0.5% potassium hydroxide) at room temperature for several hours or overnight. Stained samples were stored in 80% glycerol and photographed. For visualization of the cartilage in whole mouse embryos (E14.5), embryos were fixed in 95% ethanol overnight and stained with Alcian blue solution (80% ethanol, 20% acetic acid containing 0.1% Alcian blue) for 24 h. They were then washed for 24 h in 95% ethanol. Cartilages were cleared with 1% KOH. Embryos were stored in 80% glycerol/1% KOH.

Positional cloning

The *bis* heterozygous fish maintained on the southern Cab genomic background were mated with the wild-type northern HNI fish to generate F1 families. Embryos for the genetic mapping were obtained from inter-crosses of the F1 *bis* carriers. For establishment of the initial genetic linkage, bulk segregant analysis was conducted on pools of genomic DNA from the *bis* mutants and wild-type embryos by using the sequence-tagged site (STS) markers on the medaka genome (Kimura et al., 2004). The genetic interval was narrowed down by the analysis of individual embryos by the use of additional STS markers, MF01SSA007H10 and MF01SSA044E03 (Naruse et al., 2000), and newly designed restriction fragment length polymorphism (RFLP) markers, CRELD and BICD2 [CRELD, 5′-AGATAGAAGACCAAGTGGAGACG-3′ and 5′-GTATCCTGGATCGCAGATGC-3′/HinfI; and BICD2, 5′-TCTGCGGACAGTCCTAAAGG-3′ and 5′-TTGGACAGAGCAATCTCAGC-3′/HhaI]. cDNAs of *brpf1* from the *bis* mutants and the wild types were amplified in 2 groups of about 2000 base pairs (bps) and the sequences verified. To directly confirm the linkage between the *bis* locus and *brpf1*, we amplified a part of *brpf1* genomic DNA (primers 5′-GCTAAGGACACGGTGTTTTAC-3′ and 5′-GCTGCCTGGTACCATCTGTC-3′), and digested the PCR fragments with the restriction enzyme DdeI, which cleaves the mutant-type allele, but not the wild-type one. The nucleic acid sequence of medaka *brpf1* was deposited in the DDBJ/EMBL/GenBank. Accession No. AB488461.

Immunohistochemistry

Embryos were fixed with 4% paraformaldehyde/PBS for 2 h. After fixation, embryos were washed three times for 10 min each time with MABT (0.1% Triton-X-100 in MAB, which was 100 mM maleic acid and 150 mM NaCl, pH 7.5) and subsequently with MABDT (1% BSA and 1% DMSO in MABT) twice for 30 min each time. After having been blocked with 2% lamb serum in MABDT, embryos were incubated in the blocking solution containing the primary antibody (1:200; anti-Phospho-histone H3; Upstate) overnight at 4 °C. Embryos were

washed with MABDT three times for 5 min each time, four times for 30 min each time with 2% lamb serum in MABDT for blocking. Thereafter, embryos were incubated with the secondary antibody (1:1000; Alexa-488 conjugated anti-rabbit IgG; Molecular Probes) overnight at 4 °C. Then, embryos were washed with MABT and observed using a confocal microscope (Fluoview FV1000, Olympus).

Generation of construct and transgenic lines

A genomic fragment containing the *brpf1* promoter and Brpf1 coding sequence was amplified in 2 parts (5′ half and 3′ half fragments) from a BAC clone (ola14SH10) by using the appropriate primers. The amplified fragments were cloned into the TA cloning vector. We then digested the 5′-half fragment with SalI and NotI, and subcloned it into the XhoI NotI sites of an I-SceI backbone vector, which contains two I-SceI sites (Thermes et al., 2002). The 3′-half fragment, digested with NcoI and NotI, was cloned into the NcoI site of the inserted 5′-half fragment and the NotI site of the vector. This plasmid was digested with I-SceI (New England Biolabs), and the fragments (20 ng/μl) were injected into the cytoplasm of 1-cell stage embryos. The embryos showing a transiently strong expression of the exogenous gene were allowed to grow to adulthood. We then checked the GFP expression in the next generation, and picked an embryo with stable integration of the injected construct as the transgenic line.

Determination of the genotype of the rescued *bis* mutant was performed by using ENU-induced polymorphism, which exists at the genomic region 70 kb separated from the *brpf1* mutation point. This polymorphism showed strong linkage with the *brpf1* mutation (0 recombinations per 980 meioses). It was difficult to use the *brpf1* mutation point itself for determining the genotype because of the rescue construct containing the wild-type *brpf1* sequence. The genomic fragment was amplified by using the following primers: forward, 5′-ACTTCTTCTGCTTCACATGTGAC-3′, and reverse, 5′-AGAGA-CAGTCCTGGTATTCGG-3′, and sequenced by means of direct sequencing for determination of the genotype.

Whole-mount in situ hybridization of mouse embryos

Whole-mount *in situ* hybridizations were carried out according to the established protocol (Kondo and Dobbie, 2000), using DIG-labeled riboprobes. Embryos were permeabilized with 10 μg/ml proteinase K for 15 min. Probes (*Hoxa3* (Manley et al., 2004), *Hoxa4* (Lawrence et al., 2002), *Hoxd10* (Kondo et al., 1992), *Hoxd11* (Izpisua-Belmonte et al., 1991)) were described previously.

Results

Isolation of a medaka mutant that exhibits pharyngeal cartilage homeosis

To investigate organogenesis of vertebrates, we performed a medium-scale screening of medaka mutants obtained by ENU

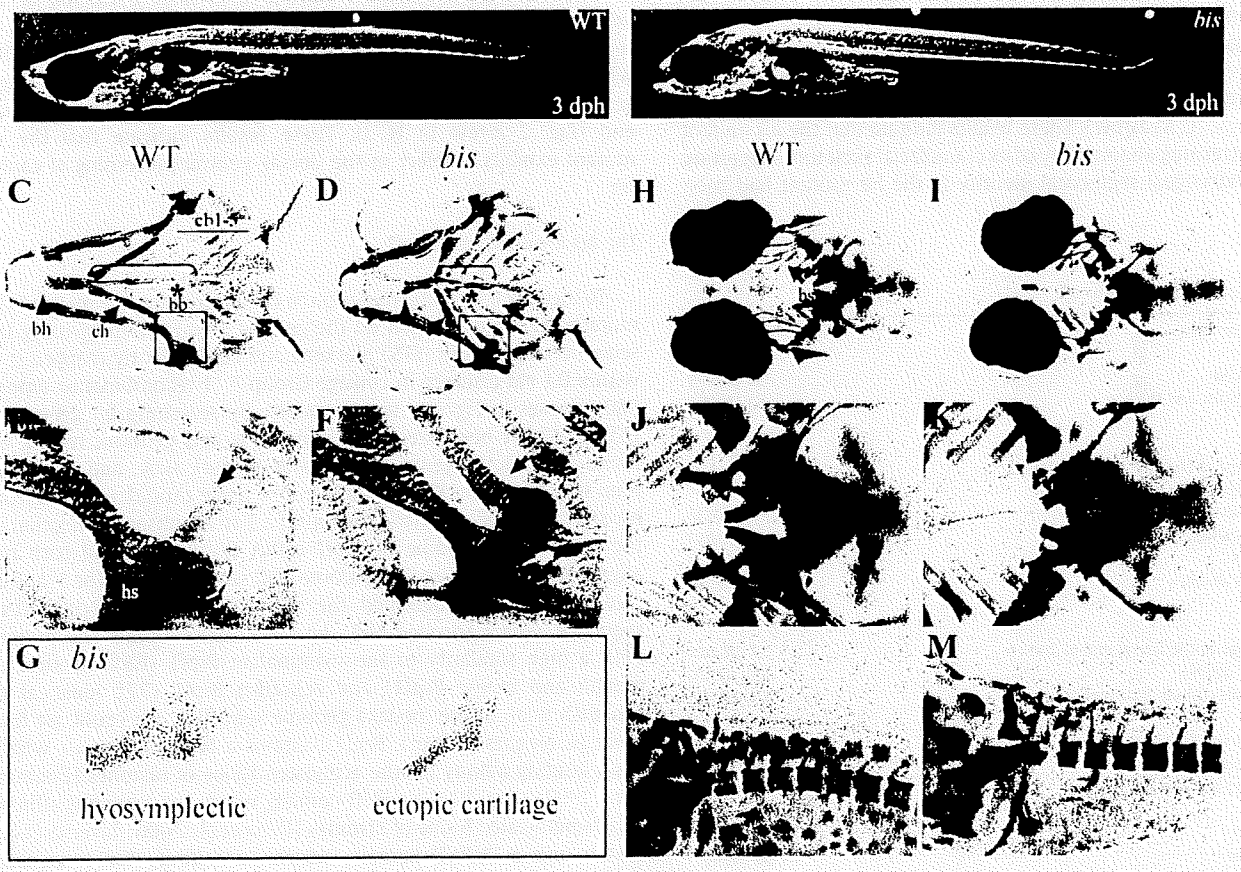

Fig. 1. The *bis* mutant displayed skeletal malformation. (A, B) Lateral view of a 3 dph larva. The *bis* mutant has a shrunken head. Other tissues appeared to have a normal morphology. (C–G) Craniofacial cartilage stained with Alcian blue. (C, D) Ventral view of wild-type and *bis* larvae. The bracket indicates the head region of the *bis* mutant and wild-type. Arrowheads indicate basihyal, which is decreased in the *bis* mutant; and arrows, the ceratohyal, which is short and thick in the mutant. (E, F) Highly magnified view of black boxed region in "C" and "D". The arrow in "F" indicates the ectopic cartilage at the lateral end of the first ceratobranchial in the *bis* mutant, compared with the wild-type (arrow in "E"). (G) View of a flat-mounted hyosymplectic and the ectopic cartilage of the *bis* mutant. The shape of ectopic cartilage has features characteristic of the hyosymplectic. (H–M) Calcified bone was stained with Alizarin red. (H, I) Ventral view of the wild type and the *bis* mutant. Arrows indicate the branchiostegal rays, which are decreased in number in the *bis* mutant. (J, K) Highly magnified view of the tooth region. Arrows indicate this region, where small pharyngeal teeth are seen in the *bis* mutant. (L, M) Lateral–dorsal view of the neck region. Arrows indicate the first vertebra, which is fused to the head in the *bis* mutant. bh, basihyal; ch, ceratohyal; cb 1–5, first to fifth ceratobranchial; bb, basibranchial; hs, hyosymplectic; bsr, branchiostegal ray; pt, pharyngeal tooth.

mutagenesis, and isolated the medaka mutant *biaxial symmetry* (*bis*). The *bis* mutant dies several days after hatching. Morphological examination showed the *bis* mutant to have a shrunken head (Figs. 1A, B). To visualize the craniofacial skeleton, we stained medaka larvae at 3 days post hatching (dph) with Alcian blue for cartilage. The craniofacial cartilage of the *bis* mutant was shrunk compared with that of the wild-type larvae (Figs. 1C, D). In the *bis* mutant, the length of each gill cartilage (ceratobranchials) was shorter, and the basihyal (derived from the second pharyngeal arch) was shortened compared with that of the wild-type larva (Figs. 1C, D, arrowhead and brackets). The ceratohyal (derived from the second pharyngeal arch) was shorter and thicker than that of the wild type (Figs. 1C, D, arrow). The second to the fifth ceratobranchials in the *bis* mutant were thicker and longer than those in the wild-type larvae (Figs. 1C, D). Although the basibranchial was separated in 2 parts in the wild-type larvae at the third ceratobranchial, the basibranchial was fused and extended to the fifth ceratobranchial in the *bis* mutant (Figs. 1C, D, asterisk). In addition, an ectopic cartilage was detected at the lateral end of the first ceratobranchial (derived from the third pharyngeal arch) on both sides of the head (Figs. 1C, D, square; E, F, arrow). An ectopic cartilage was often observed at the lateral end of the second ceratobranchial (Figs. 1C, D and Table 1). To further characterize the abnormalities of the *bis* mutant, we focused on the shape of the ectopic cartilage at the lateral end of the first ceratobranchial in the *bis* mutant. A flat-mounted observation revealed that the shape of the ectopic cartilage had the characteristic feature of the hyosymplectic, which is normally derived from the second pharyngeal arch (Fig. 1G). To observe the calcified bone, we stained the larvae with Alizarin red. Deformed brachiostegal rays (Figs. 1H, I arrow) and small pharyngeal teeth (Figs. 1J, K, arrow) were observed in the *bis* mutant. In the cervical region, the vertebra with neural arch was fused to the head skeleton in the *bis* mutant (Figs. 1L, M arrow). These results indicate that the *bis* mutant exhibits patterning abnormality of its craniofacial skeleton, suggesting that the pharyngeal segmental identity in the *bis* mutant had been disrupted.

Table 1
Skeletal phenotype of the *bis* mutant.

Cranio facial cartilage	n = 83
Arch2	
Basihyal reduced	83 (100%)
Ceratohyal shorter and thicker	83 (100%)
Arch3	
Ectopic cartilage at the lateral end of 1st cb	83 (100%)
Ectopic cartilage shape	
Small fragment	5 (6.0%)
Simple stick shape	16 (19.2%)
Similar to hs	62 (74.7%)
Hyobranchials absent	83 (100%)
Posterior arch	
Ectopic cartilage at the lateral end of 2nd cb	17 (20.4%)
Hyobranchials absent	83 (100%)
Ceratobranchials distally broadened	83 (100%)
Cervical and pharyngeal bone	n = 32
Fused vertebrate to head bone	28 (87%)
Reduced pharyngeal tooth	32 (100%)
Caudal skeleton	n = 50
Fused vertebrae	38 (76%)
Extra vertebra at the end of notochord	46 (90%)
Dorsally formed fin rays	50 (100%)
Reduced hypurals	43 (86%)

Percentage of animals with each phenotype was listed. Phenotypes of craniofacial cartilages were assessed by Alcian blue staining at 3 dph. Phenotypes of cervical and pharyngeal bone were assessed by Alizarin red staining at 3 dph and those of caudal skeletons were assessed by Alizarin red staining at 4 dph. These phenotypic differences of caudal skeleton were most likely caused by the subtle difference of the developmental stage in each animal.

The bis mutant exhibits defective skeletal patterning at the posterior region

The *bis* mutant exhibited disruption of the skeletal patterning not only in the anterior head region, but also in the posterior region. Compared with those of the wild-type larvae, the fin rays were ectopically formed at the dorsal region of caudal fin in the mutant (Figs. 2A, B, arrow); and the ossification pattern was disrupted at the caudal vertebrae in the *bis* mutant. An extra vertebra had formed at the end of the notochord in the *bis* mutant (Figs. 2A, B, arrowhead). In addition, the ossified hypural in the *bis* mutant was smaller than that of the wild type, and the hypural of the caudal most vertebra was deleted in the *bis* mutant (Figs. 2A, B, asterisk). Morphological analyses of embryos stained with Alcian blue revealed that the hypural was also ectopically formed at the dorsal side of the caudal fin and that each hypural was fused in the *bis* mutant (Figs. 2C, D, arrow). Furthermore, the blood vessels were ectopically extended at the dorsal side of the caudal fin in the *bis* mutant at 7 dpf (Fig. 2F, arrow) as opposed to their normal pattern in the wild type (Fig. 2E, arrow). To further characterize the caudal 287 fin abnormality of the bis mutant, we examined mitotic cells using mitotic marker phospho-histone H3 antibody at day 7 post fertilization (7 dpf), because the mesenchyme of the caudal fin, which exists at the ventral caudal end of the notochord, is known highly proliferative and involved in the development of the caudal fin (Hadzhiev et al., 2007; Sakaguchi et al., 2006). In the wild-type larvae, the mitotic cells largely existed at the ventral caudal end of the notochord (Fig. 2 arrow in G, I), as reported previously (Hadzhiev et al., 2007; Sakaguchi et al., 2006); whereas in the *bis* mutant, the mitotic cells existed not only at the ventral caudal end of the notochord but also at the dorsal caudal end (Fig. 2 arrow in H, I). These results indicate that the *bis* mutant exhibits a defect in the dorsal–ventral patterning of caudal fin.

The bis locus encodes brpf1

To identify a genomic mutation in the *bis* mutant, we mapped the mutated genomic position on the genetic linkage map by using the sequence-tagged site (STS) markers, and subsequently mapped it to within 0.1 cM distance in Linkage Group 7 (1 recombination among 980 meioses in Fig. 3A; see Methods). By searching for genes and ESTs that have been previously mapped to this genomic region, we found 3 predicted genes homologous to *fgd1*, *wnk*, and *brpf1*. We then sequenced the RT-PCR fragment of these candidate genes from *bis* and wild-type embryos, and found a T to A nonsense mutation in the open reading frame of *brpf1* cDNA (Fig. 3B). Using both the alignment of vertebrate Brpf1 amino acid sequences and the 5′ and 3′ race methods, we identified the medaka full-length *brpf1* cDNA sequence, which encoded 5451 bp and a 1283 amino acid protein with a high similarity to the mammalian Brpf1 (68% identical to human and mouse Brpf1) and zebrafish Brpf1 (77% identical to zebrafish one). In the medaka genome sequence, we could not find other paralogues of Brpf1. Brpf1 contains a BROMO domain, which has a binding affinity for the acetylated lysine of histones (Dhalluin et al., 1999; Yang, 2004); a PHD domain, which has a binding affinity for tri-methylated lysine of histones (Peña et al., 2006; Taverna et al., 2006); and a PWWP domain, which has affinity for condensed chromosomes (Laue et al., 2008; Turlure et al., 2006). In the *bis* mutant, the T to A transition introduced a stop codon (Y810Stop) at the end of BROMO domain, resulting in a truncated form of Brpf1 (Figs. 3B, C).

To examine the expression pattern of *brpf1*, we performed whole-mount RNA *in situ* hybridization on medaka embryos. The expression of *brpf1* was ubiquitous at st 21 (Fig. 3D), whereas at st 30 it was decreased in the trunk region and expressed in the